MICROCOPY RESOLUTION TEST CHART

NATIONAL BUREAU OF STANDARDS-1963-A

AD-A170 899

		PAGE	READ INSTRUCTIONS BEFORE COMPLETING FORM
1. REPORT NUMBER AFIT/CI/NR 86-67T	2. GOVT ACCESSION NO.	3. RECIPIENT'S CATALOG NUMBER	
4. TITLE (and Subtitle) Modification of Parameterized Latent Heat Release Estimates Using Unenhanced and Enhanced Satellite Imagery		5. TYPE OF REPORT & PERIOD COVERED THESIS/DISSERTATION	
		6. PERFORMING ORG. REPORT NUMBER	
7. AUTHOR(s) William F. Sjoberg		8. CONTRACT OR GRANT NUMBER(s)	
9. PERFORMING ORGANIZATION NAME AND ADDRESS AFIT STUDENT AT: Purdue University		10. PROGRAM ELEMENT, PROJECT, TASK AREA & WORK UNIT NUMBERS	
11. CONTROLLING OFFICE NAME AND ADDRESS AFIT/NR WPAFB OH 45433-6583		12. REPORT DATE 1986	
		13. NUMBER OF PAGES 100	
14. MONITORING AGENCY NAME & ADDRESS(if different from Controlling Office)		15. SECURITY CLASS. (of this report) UNCLAS	
		15a. DECLASSIFICATION/DOWNGRADING SCHEDULE	

16. DISTRIBUTION STATEMENT (of this Report)

APPROVED FOR PUBLIC RELEASE; DISTRIBUTION UNLIMITED

DTIC
ELECTE
AUG 1 3 1986
S
B
D

17. DISTRIBUTION STATEMENT (of the abstract entered in Block 20, if different from Report)

18. SUPPLEMENTARY NOTES

APPROVED FOR PUBLIC RELEASE: IAW AFR 190-1

LYNN E. WOLAVER 6 AUG 86
Dean for Research and
Professional Development
AFIT/NR

19. KEY WORDS (Continue on reverse side if necessary and identify by block number)

20. ABSTRACT (Continue on reverse side if necessary and identify by block number)

ATTACHED.

DD FORM 1473 EDITION OF 1 NOV 65 IS OBSOLETE
1 JAN 73

86   8   12   014

Woodley,W.L.,A.R. Olsen,A. Herndon ,and V. Wiggert, 1975: Comparison of gage and radar methods of convective rain measurement. J.Appl.Meteor.,14, 909-928.

_____,C.G. Griffith,J.S. Griffin, and S.C. Stromatt, 1980: The influence of GATE convective rainfall from SMS-1 imagery. J.Appl.Meteor.,19, 388-408.

This study investigates the use of unenhanced and enhanced satellite imagery to modify parameterized latent heat release for a developing cyclone over the central United States during 10-11 April 1979. Parameterized stable and convective latent heat release estimates are evaluated initially by a qualitative comparison with National Weather Service radar summaries; gridded, time-averaged observed precipitation fields; and satellite-derived cloud cover. This evaluation is then extended to the latent heating values obtained after applying the three modification schemes. Finally, the latent heating values are evaluated quantitatively using the gridded, observed precipitation values. This evaluation includes comparisons of area-averaged totals and correlation coefficients for the total SESAME grid. In addition, the total number of grid points at which observed precipitation and latent heating values occurred over both the total SESAME grid and three subregions representing different air mass regions are compared.

Results indicate that the satellite schemes yield improved latent heat release estimates. This is seen in the improved areal coverage of modified latent heat release fields when compared with radar and observed precipitation summaries. In addition, a 21%-45% improvement in the average correlation between calculated LHR and observed precipitation values is obtained. Furthermore, the number of grid points at which LHR was calculated matches the observed precipitation grid points more closely after the modifications were applied. When the three modifications are compared, it is seen that there is considerable support for identifying the second modification as yielding the best match between latent heat release values and the comparative data forms. This modification uses a $235^\circ K$ threshold to differentiate between convective and stable regions of a cloud mass. It was also found that the impact of these modifications varies depending on the accuracy of the initial latent heat release calculations.

PURDUE UNIVERSITY

Graduate School

This is to certify that the thesis prepared

By ___William Frances Sjoberg_____

Entitled

Modification of Parameterized Latent Heat Release Estimates Using
Unenhanced and Enhanced Satellite Imagery

Complies with University regulations and meets the standards of the Graduate School for
originality and quality

For the degree of ___Master of Science_____

Signed by the final examining committee:

_____ , chair

_____

_____

Approved by the head of school or department:

April 25 19_86_ _____

☐ is
This thesis ☒ is not to be regarded as confidential

_____
Major professor

MODIFICATION OF PARAMETERIZED

LATENT HEAT RELEASE ESTIMATES USING

UNENHANCED AND ENHANCED SATELLITE IMAGERY

A Thesis

Submitted to the Faculty

of

Purdue University

by

William Francis Sjoberg

In Partial Fulfillment of the

Requirements for the Degree

of

Master of Science

May 1986

ACKNOWLEDGEMENTS

I am indebted to Professor Phillip J. Smith for proposing this work and for his advice and patience during the course of my studies. His assistance and guidance were instrumental to the successful completion of my research and this thesis. I am also grateful to Professor Dayton G. Vincent and Professor John T. Snow for serving on my committee and for expending considerable time and effort to assist me in this endeavor.

I would like to thank Doctor Franklin R. Robertson for providing the satellite imagery used in this study, as well as his insights into how best to use this data. A special thanks goes to Doug Miller for the many hours he spent drafting the figures in this study. Without his quick and steady hand this work would have taken much longer. I would also like to thank the students and staff of the Geosciences Department who have provided a relaxed and enjoyable environment in which to work.

TABLE OF CONTENTS

LIST OF TABLES

LIST OF FIGURES

ABSTRACT

Sjoberg,William F.,M.S., Purdue University, May 1986.
Modification of Parameterized Latent Heat Release
Estimates Using Unenhanced and Enhanced Satellite Imagery.
Major Professor: Dr. Phillip J. Smith

This study investigates the use of unenhanced and
enhanced satellite imagery to modify parameterized latent
heat release for a developing cyclone over the central
United States during 10-11 April 1979. Parameterized
stable and convective latent heat release estimates are
evaluated initially by a qualitative comparison with
National Weather Service radar summaries; gridded, time-
averaged observed precipitation fields; and satellite-
derived cloud cover. This evaluation is then extended to
the latent heating values obtained after applying the
three modification schemes. Finally, the latent heating
values are evaluated quantitatively using the gridded,
observed precipitation values. This evaluation includes
comparisons of area-averaged totals and correlation
coefficients for the total SESAME grid. In addition, the
total number of grid points at which observed
precipitation and latent heating values occurred over both
the total SESAME grid and three subregions representing

different air mass regions are compared.

Results indicate that the satellite schemes yield improved latent heat release estimates. This is seen in the improved areal coverage of modified latent heat release fields when compared with radar and observed precipitation summaries. In addition, a 21%-45% improvement in the average correlation between calculated LHR and observed precipitation values is obtained. Furthermore, the number of grid points at which LHR was calculated matches the observed precipitation grid points more closely after the modifications were applied. When the three modifications are compared, it is seen that there is considerable support for identifying the second modification as yielding the best match between latent heat release values and the comparative data forms. This modification uses a 235°K threshold to differentiate between convective and stable regions of a cloud mass. It was also found that the impact of these modifications varies depending on the accuracy of the initial latent heat release calculations.

1. INTRODUCTION

Relationships between atmospheric circulation systems and latent heat release occurring during cloud/precipitation formation have been a matter of major concern in meteorology for a number of years (e.g., Aubert, 1957; Danard, 1964,1966; Tracton,1973; Vincent et al.,1977; Robertson and Smith,1983; Gyakum, 1983a,b; Smith et al.,1984). A typical diagnosis of latent heat release involves partitioning the quantity into two components, stable(grid-scale) and convective (subgrid-scale). The stable component is generally determined as a function of the grid-scale vertical motion and the vertical gradient of water vapor. Methods of quantifying the convective component have concentrated on two approaches. The first approach focuses on the microphysical processes of individual cumulus clouds or cloud ensembles. Schemes utilizing this approach have been advanced by Kessler(1969), Simpson and Wiggert(1971), Takeda(1971), and Orville and Kopp(1977). The second approach centers on the parameterization of subgrid-scale(cumulus) processes using available grid-scale information ,e.g., parameterizations by Kuo(1965,1974), Ooyama(1971), Arakawa

and Chao(1973), and Krishnamurti and Moxim(1971). A general discussion and comparison of the various cumulus parameterization schemes can be found in Ceselski(1973) and Krishnamurti et al. (1980). The scheme used in this study was introduced by Kuo(1965,1974), and later modified by Edmon and Vincent(1976) and Lin and Smith(1979).

Although much has been done to produce realistic latent heat estimates, diagnostic studies to date reveal deficiencies in both the magnitudes and the distribution of latent heating values. Since latent heating is closely tied to the occurrence of clouds and precipitation, information about the latter provides independent data which can be used to improve previously obtained estimates of latent heating. In this context, earth orbiting satellites are particularly useful because they provide platforms for estimating cloud conditions over large areas. Further, as suggested by Barrett(1970,1971), satellite data can be used to estimate rainfall amounts. Thus, it should be possible to use satellite information to improve latent heat release estimates.

There has been considerable work done on the use of satellite data to estimate rainfall amounts. Barrett and Martin(1981) divided these methods into three categories: 1) cloud-indexing methods, (Barrett, 1970,1971); 2) life-history methods, (Griffith et al., 1976, 1978; Woodley et al., 1980; Scofield and Oliver, 1977); and 3) passive-

microwave methods, (Wilheit, 1972; Smith and Kidder, 1978). Each of these methods acknowledges the importance of accurate satellite cloud estimations.

In the present study the utilization of satellite data is taken to its next logical step, that of combining direct estimates of latent heating with satellite data in order to compensate for the inherent deficiencies contained in each. Latent heat release calculations are easily made from the synoptic-scale data network, yet can suffer from inadequate data coverage, erroneous data, and/or computational model deficiencies. Satellite data give spatially complete and detailed views of cloud distributions, but do little to account for the large changes in rainfall found in small regions of convective clouds, precipitation variations that can occur within similarly appearing cloud fields, or the vertical distribution of the resulting latent heat release.

The work presented here is an extension of the simple technique described by Lin and Smith(1985), in which calculated latent heating is modified using satellite-derived cloud information. Using enhanced infrared satellite imagery, the Lin and Smith procedure is refined in two ways, one to permit the discrimination between stable and convective cloud forms and the other to allow a determination of the heights of satellite-derived cloud tops.

The objectives of this research are 1) to compare the parameterized latent heat release estimates obtained from the SESAME I data set with observed precipitation values and radar fields, 2) to test three procedures for utilizing satellite cloud images to modify these conventional latent heating estimates, and 3) to propose a procedure which combines latent heat release calculations and satellite imagery and whose results exhibit the best comparison with observational data forms.

2.   DATA AND COMPUTATIONS

2.1 Rawinsonde data

The period of investigation consists of seven synoptic times, 3h apart, from 1200GMT 10 April through 0600GMT 11 April 1979. These times were chosen to correspond to a much publicized outbreak of severe weather in the central United States. An extratropical cyclone with significant convective activity and associated latent heat release was observed by the special data network initiated for the AVE-SESAME (Atmospheric Variability Experiment-Severe Environmental Storms and Mesoscale Experiment) field program. The network consisted of 23 National Weather Service (NWS) and 16 supplementary rawinsonde sites (Fig.2.1), with observations taken at 3h intervals over a 24h period from 1200GMT 10 April - 1200GMT 11 April 1979, a period commonly known as SESAME I. Further details of the AVE-SESAME '79 experiment are given by Alberty et al. (1979), Hill et al. (1979), and Gerhard et al. (1979).

The observational data set included geopotential height, temperature, relative humidity, horizontal wind components, and surface pressure. These data were then

Figure 2.1. SESAME I upper air data network showing locations of 23 National Weather Service and 16 supplementary rawinsonde stations. Stations with numbers 19 or less are supplementary.

Figure 2.1.

objectively analyzed using the Barnes (1964,1973) scheme on a 12 X 18 latitude/longitude grid with one degree latitude/longitude resolution (Fig.2.2). All data were interpolated to 50 mb levels extending from 1000 mb to 100 mb. Including the surface, this gave a total of 21 levels of data. The gridded data set was provided to the author by Dr. F. R. Robertson of the NASA Marshall Space Flight Center.

Vertical motions were estimated from horizontal wind components by the kinematic method, which utilizes the continuity equation in pressure coordinates (O'Brien, 1970). Because there are systematic errors inherent in the evaluation of divergence fields, unrealistically large estimates of ω are often produced at the upper levels. Such bias errors were suppressed by the quadratic adjustment scheme suggested by O'Brien (1970) and applied by Smith (1971).

2.2 Precipitation data

Observed precipitation rates, used to evaluate the vertically integrated values of parameterized latent heat release, were obtained from the Hourly Precipitation Data booklets published by the National Climatic Data Center, NOAA. Precipitation data were smoothed to the grid by averaging reported precipitation quantities over each one
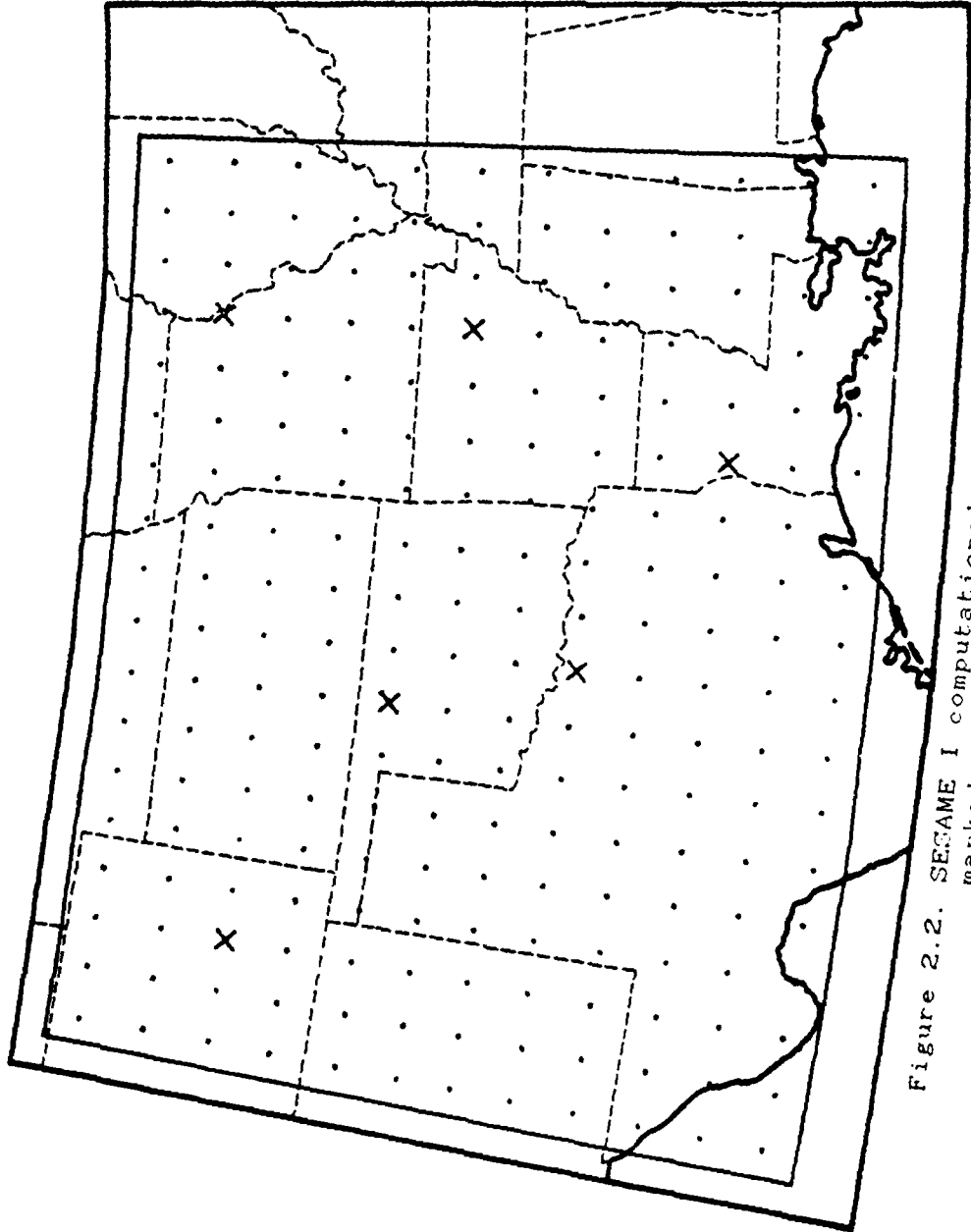
Figure 2.2. SESAME I computational grid. Grid points marked with an x are those where upper air soundings were done in section 2.4.4.

degree grid square for 3h periods, i.e., 1h before to 2h after the seven synoptic times under consideration. These data were provided to the author by Dr. D. G. Vincent, Department of Geosciences, Purdue University.

2.3 Calculation of latent heat release

Convective latent heat release (CLHR) was computed using Kuo's (1965,1974) parameterization scheme as modified by Edmon and Vincent (1976) and Lin and Smith (1979). Stable latent heat release (SLHR) was evaluated from a scheme used by Krishnamurti and Moxim (1971). Both heating components were allowed to occur simultaneously in the same region.

In the Kuo scheme the CLHR is parameterized by:

$$CLHR = \frac{g(1-b)L \, M_t [\, T_c(p) - T(p)\,] \, \theta/T}{(p_b - p_t) < T_c - T >} \qquad (1)$$

for those levels with $T_c > T$, where

$$bM_t = \frac{1}{g} \int_{p_u}^{p_0} \frac{\partial q}{\partial t} \, dp \quad ,$$

$$< T_c - T > = \frac{1}{p_b - p_t} \int_{p_t}^{p_b} (\, T_c - T \,) \, dp \quad ,$$

M_t = the rate of moisture convergence from the surface to the cloud top, including horizontal convergence of specific humidity and evaporation of water from the lower surface;

T = the environmental temperature;

T_c = the temperature within the cloud, assumed to be the temperature of the moist adiabat extending from the cloud base;

θ = the potential temperature;

L = the latent heat of condensation,

= 2.501×10^6 JKg^{-1} for $T \gtrsim -20°$ C,

= 2.835×10^6 JKg^{-1} for $T < -20°$ C;

p_b = the pressure at the cloud base, the base of the first conditionally unstable layer;

p_t = pressure at the cloud top, the level at which the moist adiabat from the cloud base crosses the environmental sounding; and

b = the fraction of M_t stored in the air to increase the specific humidity of the environment.

The Kuo scheme contains the following modifications (Edmon and Vincent,1976; Lin and Smith,1979). A latent heating value was calculated only if 1) the cloud was at least 100 mb in depth, 2) the mean vertical motion within the cloud layer was upward, and 3) the mean relative humidity between the surface and 500 mb (RH_{av}) was greater than 0.4. The partitioning parameter b was evaluated as a

function of RH_{av} in a fashion similar to Anthes(1977) and Donner and Kuo(1982). If the value of RH_{av} was less than or equal to 0.4, then b was assumed to be one (i.e., no convective latent heat release). If RH_{av} was greater than or equal to 0.8, then b was assumed to be zero. This upper bound corresponds with the relative humidity constraint imposed on the stable precipitation. If RH_{av} was between 0.4 and 0.8, b was assumed to be $1-RH_{av}$.

SLHR was calculated from the equation,

$$SLHR = -L\omega \frac{\partial q_s}{\partial p}, \qquad (2)$$

where ω is the vertical velocity in pressure coordinates and q_s is the saturated specific humidity. Stable latent heat release was specified under the following limitations; 1) grid-scale upward vertical motion, 2) vertical moisture convergence for saturated air at environmental temperatures, 3) relative humidity greater than or equal to 80% (Krishnamurti and Moxim, 1971; Edmon and Vincent, 1976).

Henceforth, the sum of CLHR and SLHR will be identified as total latent heat release (TLHR). Results obtained from these calculations are referred to as the "basic" latent heat release (BLHR).

2.4 <u>Modification of latent heat calculations</u>

Satellite images were obtained for the seven time periods under consideration. The modification schemes were based on both unenhanced and enhanced infrared satellite images. Only IR data were used in order to standardize the modification schemes for use during both day and night. Using the basic analysis grid described earlier, each grid square was assigned a satellite-derived cloud fraction based on the percent cloud cover estimated for that square. The satellite cloud fraction value was used to modify the basic latent heat estimates. Earlier work done by Lin and Smith(1985) describes the use of unenhanced satellite data to modify latent heat release calculations. This study applies their technique to the SESAME I case and extends their work by including enhanced satellite data.

2.4.1 Description of satellite cloud data

All satellite images were derived from the SMS-1 satellite observing system and were provided to the author by the NASA Marshall Space Flight Center. During the SESAME I period the SMS-1 was in a geosynchronous orbit at an approximate altitude of 35800km over the equator and was located at a fixed longitude of 75°W. The SMS-1 was equipped with a visible and an infrared spin scan

radiometer(VISSR) which scans the full disc of the earth in 18.2 minutes, viewing in the visible spectrum (0.55 to 0.75μm) and in the infrared spectrum(10.5 to 12.6μm). Visible and infrared data resolutions are approximately 4km at the satellite subpoint. Subsequent sections will discuss the logic behind the specific enhancements used in this study and how these enhancements were incorporated into the latent heat release modification schemes. More details regarding the SMS-1 satellite and its instrumentation can be found in National Space Science Data Center(NSSDC) publication: "Data Catalog Series for Space Science and Applications Flight Missions: Volume 4a," Ng and Shue editors.

2.4.2 Lin and Smith modification

Using unenhanced satellite imagery, for each grid square a satellite-derived cloud fraction value of 0, 0.5, or 1 was assigned. A value of 1 was given to those squares with over 80% of its area covered with cloud. Squares with less than 20% of its area covered with cloud were assigned a value of 0. For squares with satellite cloud coverage between 20% and 80%, a value of 0.5 was assigned. These satellite cloud fractions(α) were used to modify the original total latent heat release estimates at every grid point and level using the following procedure. If at a gridpoint(o) the original latent heat

calculation(Q_0) was non-zero, a modified latent heat estimate(Q_0^*) was determined by

$$Q_0^* = \alpha Q_0 . \qquad (3)$$

If Q_0 was determined to be zero, and $\alpha=0$, then

$$Q_0^* = 0 , \qquad (4)$$

If Q_0 was determined to be zero but $\alpha=0.5$ or 1.0, then the modified value was determined by inverse distance weighted interpolation

$$Q_0^* = \frac{\sum \dfrac{1}{d_i} Q_i}{\sum \dfrac{1}{d_i}} , \qquad (5)$$

where d_i is the distance from grid point o to a surrounding grid point i. For grid points located at least two grid squares from the computational boundary, the interpolation was done using points two grid squares in all directions, a total of 24 interpolating points. Points located one grid square from the boundary used the immediately surrounding grid points, a total of 8 interpolating points. The points located on the boundary used the 3 adjacent computational grid points.

The modification scheme was applied to the sum of the convective and stable latent heat release (TLHR) and will

be referred to in later chapters as modified latent heat release one (MLHR1).

2.4.3 235°K enhancement modification

The next step in this inquiry was an attempt to isolate the convective region of satellite cloud masses by enhancing the satellite images using 235°K as a threshold temperature. A comparison done by Arkin(1979) of 6h rainfall accumulations over the GARP Atlantic Tropical Experiment (GATE) B-scale array and fractional cloud coverage below various IR threshold temperatures, showed that the maximum correlation of these two factors occurred at 235°K. It was found that despite GATE's phase-to-phase variablity in factors such as average rainfall rate (Hudlow et al., 1979) and the mean surface wind field (Seguin et al., 1978), the relationship between rainfall and the fractional IR cloud coverage defined by this particular threshold temperature remained nearly the same throughout GATE.

Each square in the grid was divided into regions with cloud tops colder than 235°K, warmer than 235°K, or cloud free. Modifications to the basic latent heating values were made by assuming that tops 235°K or colder contained only convective latent heat release and tops warmer than 235°K contained only stable latent heat release. The

fraction of each cloud type was estimated for each grid square and was utilized to modify the basic latent heating values in the following way. In grid squares where there was less than 20% of both types of cloud, it was assumed that no latent heat release had occurred and BLHR values were set to zero. If either type of cloud filled greater than 80% of the square it was assumed that only SLHR (CLHR) occurred if the cloud top was warmer(equal to or colder) than 235°K. In this case the non-occurring basic latent heating component was set to zero. For grid squares having some tops warmer than this threshold while other tops were colder, the latent heat release values were adjusted in the following manner. If the square was covered by 20% to 80% of one type, while the percentage of cloud of the other type was less than 20%, the modified TLHR value was assumed to be half of the basic SLHR(CLHR) value if the predominant cloud top was warmer(equal to or colder) than 235°K. If there was between 20% and 80% of both types of cloud, the modified TLHR was assumed to be half of the BLHR value.

Finally, if there was greater than 20% of any type of cloud and there was no latent heat release calculated for that grid square, the initial zero values of both components were altered using the inverse distance weighted interpolation procedure summarized in the previous section and then the SLHR and CLHR values were

modified as described above. The resulting latent heat release values from this modification will be referred to in the results chapters as modified latent heat release two(MLHR2).

2.4.4 3-layer enhancement modification

The previous two schemes made no attempt to discriminate the various heights of observed clouds; both assumed that any observed cloud extended throughout the 1000 to 100 mb layer. Thus, a third modification was devised which differentiated between low, middle, and high clouds. This differentiation was accomplished by selecting three different temperature threshholds for enhancement of the infrared photographs. By focusing on the vertical extent of the cloud it was hoped that the latent heat release calculations could be modified to ensure that latent heat release was confined to levels where cloud was present.

The definitions of low, middle, and high clouds were adopted from the Weather Almanac (1977), which specifies the height ranges shown in Table 2.1. Combining these definitions with the equivalent blackbody temperatures($^\circ$K) for typical cloud levels identified by Barrett(1972), summarized in Table 2.2, a range of temperature values was identified which made it possible to separate the various

clouds by level. To test the applicability of these temperature ranges to the current data set, six grid points were chosen and vertical temperature/dewpoint soundings were anal zed for two times, 1200GMT 10 April 1979 and 0300GMT 11 April 1979. These points, identified by an X on Fig 2.2, were chosen in order that each of the air masses involved in this synoptic disturbance would be represented. Table 2.3 shows the temperature ranges observed at these points for each of the height categories specified in Table 2.1. These results show a strong resemblance to the temperature values observed by Barrett(1972). Thus, the Barrett values represent reasonable threshold temperatures for the enhancement of the IR satellite images for this data set The temperature ranges and corresponding color code for the enhanced IR images for each cloud category are summarized in Table 2.4. The significant warming at the surface over the grid late in the study period was captured by a reduction in the maximum temperature threshold used for designating low cloud.

To provide data for the latent heat modification a grid was overlayed on the color-coded satellite images and the fraction of each cloud category was estimated for each grid square. The predominant cloud level determined the final modification of latent heat release values. For example, if a grid square was covered with 50% high cloud

Table 2.1. Cloud level definitions for MLHR3.

CLOUD LEVEL	HEIGHT OF BASES(KM)
LOW	SFC to 2
MIDDLE	2 to 7
HIGH	7 to 14

Table 2.2. Equivalent blackbody temperature($^{\circ}$K) for MLHR3 cloud level determinations (from Barrett ,1972).

CLOUD LEVEL	EQUIVALENT BLACKBODY TEMP($^{\circ}$K)
LOW	280K - 300K
MIDDLE	250K - 280K
HIGH	250K

Table 2.3. Cloud level temperatures at various grid points during SESAME I.

POINT(row, column)	HEIGHT CATEGORY		
	LOW	MIDDLE	HIGH
3,13	285K	248K - 285K	248K
5,9	288K	248K - 288K	248K
7,15	283K	248K - 283K	248K
8,9	283K	243K - 283K	243K
10,3	278K	243K - 278K	243K
11,15	280K	246K - 280K	246K

Table 2.4. Temperature thresholds of satellite imagery for MLHR3.

CLOUD LEVEL	IR COLOR CODE	10 April 1979	11 APRIL 1979
		1200GMT - 0000GMT	0300GMT - 0600GMT
LOW	BLUE	280K - 300K	280K - 290K
MIDDLE	GREEN	250K - 280K	250K - 280K
HIGH	RED	250K	250K

and 20% middle cloud, the square was assumed to be covered with 70% high cloud. It was then assumed that latent heat release took place at all levels below the level of cloud designated as the predominant cloud in a grid square. If the different cloud levels covered approximently the same area of a grid square, the highest level was assumed to be the predominate cloud type. This cloud type was then designated as the type for the total percentage of grid space covered by cloud. For example, if a grid square was covered with 30% low cloud and 30% middle cloud, the square was then assumed to be covered with 60% middle cloud. With this value set, the modification of latent heating values was done using the same procedure as described in the Lin and Smith section. As before, a zero latent heat release value was assigned to squares with less than 20% of their areas covered with cloud. Also, if clouds were observed but no latent heat was calculated, the inverse distance weighted interpolation was done at each level using the initial latent heat release values. The predominant cloud type was then designated and the modification was applied. Note that, as with the original Lin and Smith procedure(MLHR1), this modification was applied to the TLHR, not to the two subcomponents seperately. The latent heat release values resulting from this modification will be referred to in the results chapters as modified latent heat release three(MLHR3).

2.5 Evaluation procedures

Initially, latent heat release values were evaluated by comparing the areal coverage of calculated latent heat release with radar summaries obtained from the National Weather Service, satellite cloud depictions, and observed precipitation fields. Additional comparisons were made by calculating area averages and correlation coefficients between the observed precipitation rates, after space and time smoothing, and the precipitation rates corresponding to the vertically-integrated values of calculated total latent heat release. Finally, areal latent heating and observed precipitation coverages over the total domain, as well as homogeneous sub-regions, were compared by simply counting the number of grid points over which precipitation was observed or LHR was calculated. All grid point observed precipitation and calculated LHR values less than $0.04mmh^{-1}$ were regarded as trace amounts and were set to zero.

3.   SYNOPTIC DISCUSSION

The basic synoptic features, with corresponding precipitation distributions, are represented by the radar depictions and superimposed surface pressure centers and fronts in Fig.3.1.   More detailed synoptic discussions have been presented for the SESAME I period by Alberty et al. (1979), Carlson et al. (1980), Moore and Fuelberg (1981), and Vincent and Homan (1983).   The following serves as a brief summary of the evolution of the cyclone and its associated precipitation field.

Synoptic conditions at 1200GMT 10 April featured a deep cyclone located over northcentral Colorado, with a cold front stretching southward through New Mexico.   During the 10th, moist air from the Gulf of Mexico was flowing northward across Texas, while dry air from eastern New Mexico pushed a dry line east and northeast across western Texas.   Early radar summaries show that rainshower and thundershower activity was confined to the region affected by a weakening upper air shortwave that was moving through the Mississippi Valley.   As the dry line moved into westcentral Texas near 1800GMT, there was a dramatic

Figure 3.1. National Meteorological Center(NMC) radar summary charts with superimposed major surface cyclone and fronts. Cloud tops in dam, motion vectors in m s^{-1}.
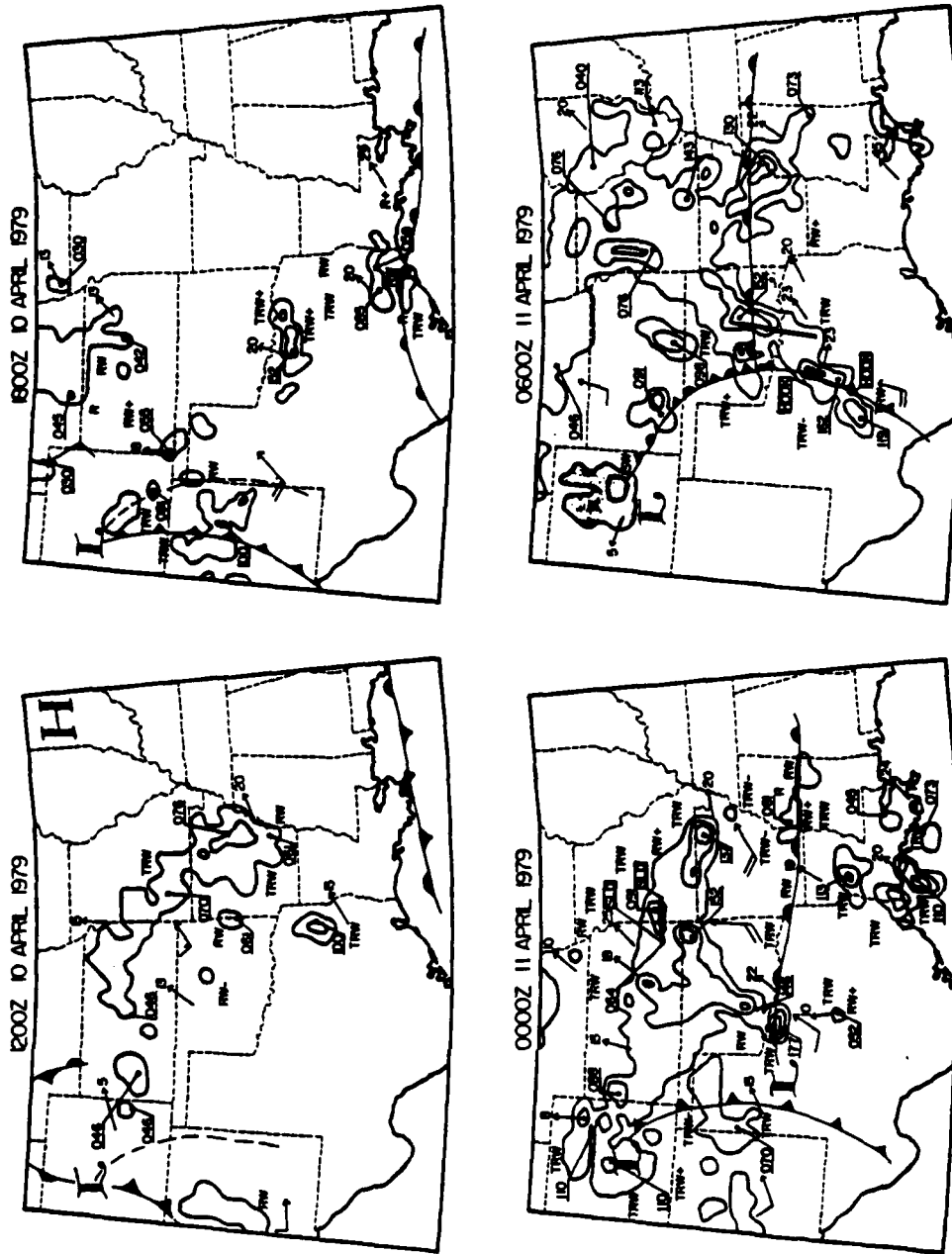
Figure 3.1.

there was a dramatic increase in the convective activity near the Texas-Oklahoma border. Fig.3.1 shows that cells with tops exceeding 15000 m were already occurring at 1800GMT.

Accompanying the synoptic-scale features was a mesoscale low which had formed in the Texas panhandle at 1500GMT, thus helping to create an environment conducive to severe weather. In addition, a cold front in New Mexico moved slowly eastward early in the study period, then accelerated rapidly as it pushed into Texas after 1800GMT.

By 0000GMT 11 April, the sporadic convective activity in the region had given way to a more organized precipitation area north of the warm front that had moved into southern Oklahoma. This organized precipitation region moved eastward by 0600GMT with the severe weather and strong convection extending into southcentral Texas in association with the cold front that moved through this region. The extensive, but weaker, area of rainshowers and thundershowers in Kansas and southern Nebraska had moved into Missouri and western Illinois. The broad area of air mass thunderstorms in the lower Mississippi Valley had begun to dissipate rapidly late in the day. Echo tops in Louisiana and Mississippi at 0600GMT were under 10000 m. The AVE-SESAME domain was favorably located to encompass the major precipitation regions of this synoptic disturbance.

4.   THE BASIC LATENT HEAT RELEASE CALCULATIONS

4.1 Horizontal distributions

As an initial step in the evaluation of the latent heat calculations, the horizontal fields of basic latent heat release(BLHR) estimates, derived from the parameterization schemes described in Chapter 2, are examined. Observed precipitation, satellite-derived cloud, radar, and BLHR fields for four map times are presented in Figs.4.1-4.4. Before proceeding with the discussion, it must be acknowledged that comparisons of these data forms are complicated by a measure of incompatability that exists between them. The radar maps depict instantaneous fields of larger water droplets, some of which are associated with subgrid-scale events. Satellite imagery allows an instantaneous view of cloud tops, but obscures the condensate that might or might not exist below.   As with the former two, BLHR values are obtained at particular times but are representative of grid-scale processes. Finally, the observed precipitation values are smoothed over three-hour periods(see Sect.2.2) to make them more compatible with the BLHR values and are subject to errors introduced by the use of different types of raingauges and

Figure 4.1. Top left: NMC radar summary chart for 1200GMT 10 April 1979. Cloud tops in dam, motion vectors in m s^{-1}.
Top right: Observed precipitation rate(mm h^{-1}) for 1200GMT 10 April 1979.
Bottom left: Satellite cloud pattern.
Bottom right: Vertically integrated basic latent heat release(BLHR) combining convective and stable components(mm h^{-1}).
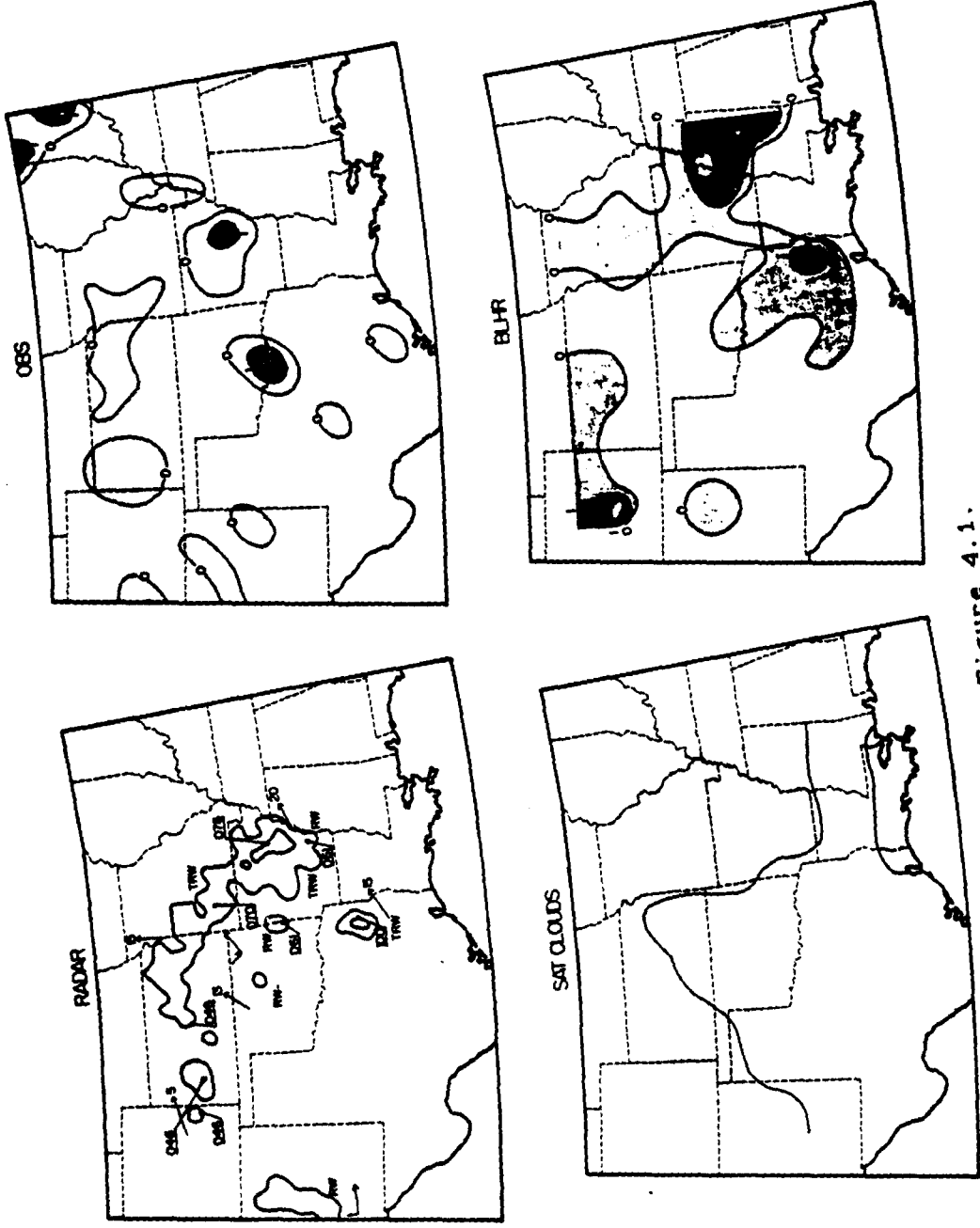
Figure 4.1.

Figure 4.2. Top left: NMC radar summary chart for 1800GMT
10 April 1979. Cloud tops in dam, motion
vectors in m s^{-1}.
Top right: Observed precipitation rate(mm h^{-1})
for 1800GMT 10 April 1979.
Bottom left: Satellite cloud pattern.
Bottom right: Vertically integrated basic
latent heat release(BLHR) combining convective
and stable components(mm h^{-1}).
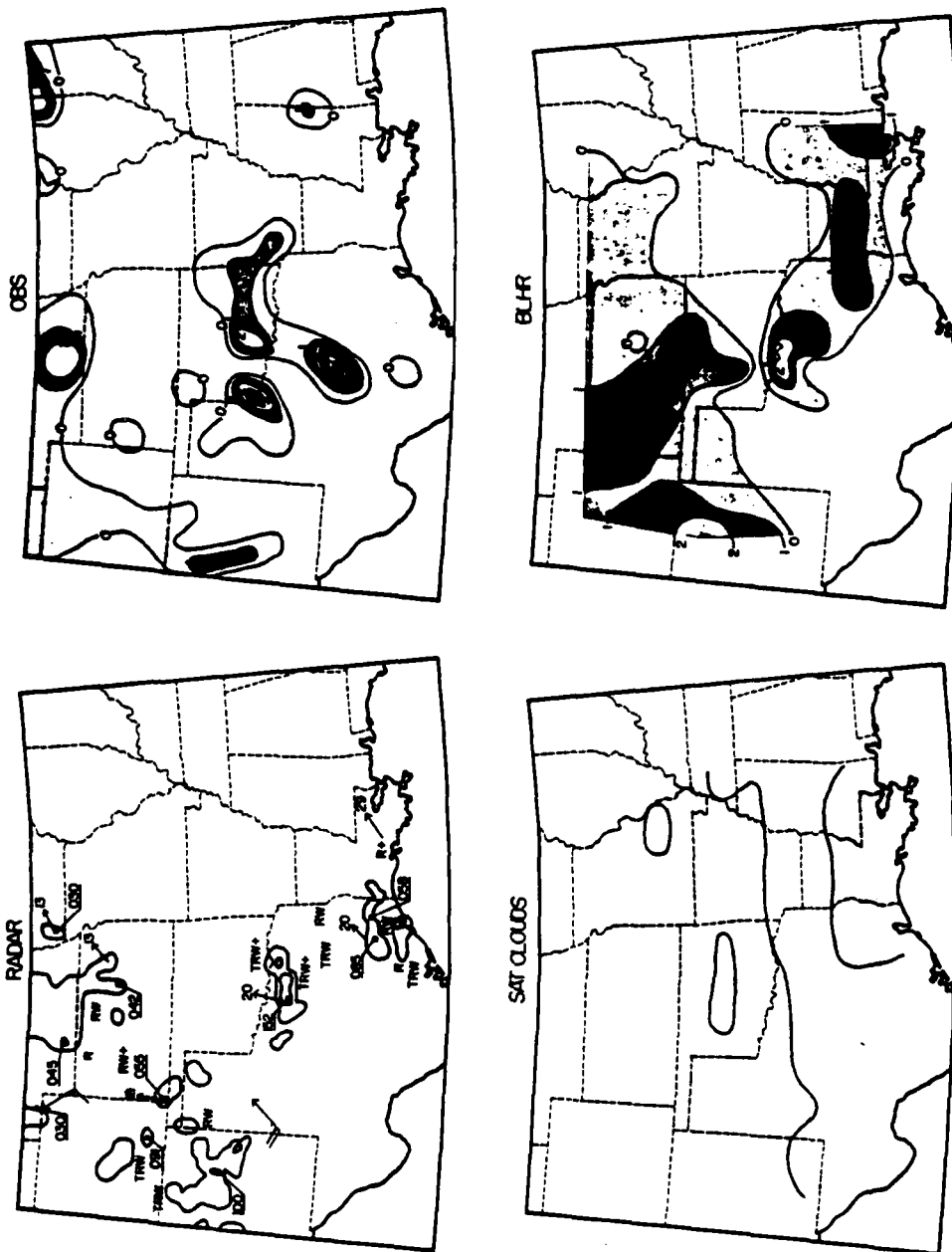
Figure 4.2.

Figure 4.3. Top left: NMC radar summary chart for 0000GMT 11 April 1979. Cloud tops in dam, motion vectors in m s^{-1}.
Top right: Observed precipitation rate(mm^{-1}) for 0000GMT 11 April 1979.
Bottom left: Satellite cloud pattern.
Bottom right: Vertically integrated basic latent heat release(BLHR) combining convective and stable components(mm h^{-1}).

Figure 4.3.

Figure 4.4. Top left: NMC radar summary chart for 0600GMT 11 April 1979. Cloud tops in dam, motion vectors in m s^{-1}.
Top right: Observed precipitation rate(mm h^{-1}) for 0600GMT April 1979.
Bottom left: Satellite cloud pattern.
Bottom right: Vertically integrated basic latent heat release(BLHR) combining convective and stable components (mm h^{-1}).

Figure 4.4.

different precipitation reporting procedures. Additional comment on raingauge density and location and its effect on area precipitation totals can be found in Woodley et al. (1975) and Hildebrand et al. (1979).

Inconsistencies between the radar and observed precipitation summaries are particularly troublesome because each represents an independent standard against which the computed latent heat release values can be compared. Several examples of such inconsistencies can be identified for this case study. At 1200GMT (Fig.4.1), an area of radar echoes in northeastern Texas does not appear on the observed precipitation summary, while observed precipitation areas in central Texas are not reflected in the radar summary. At 1800GMT (Fig.4.2), an observed precipitation pattern extending from central Texas well into eastern Oklahoma and western Arkansas is substantially larger than the radar area which is confined to northern Texas. In this latter example the precipitation area occurs in response to a rapidly expanding area of convection which spread north and east out of northcentral Texas. Interestingly, while the instantaneous radar summary does not depict this area, a combination of successive radar summaries does. This is clearly shown in Fig.4.5, which depicts the radar summaries for 1735GMT, 1835GMT, and 1935GMT. This figure also shows yet another inconsistency example, namely radar

Figure 4.5. NMC radar summary charts. Cloud
tops in dam, motion vectors in
m s^{-1}.
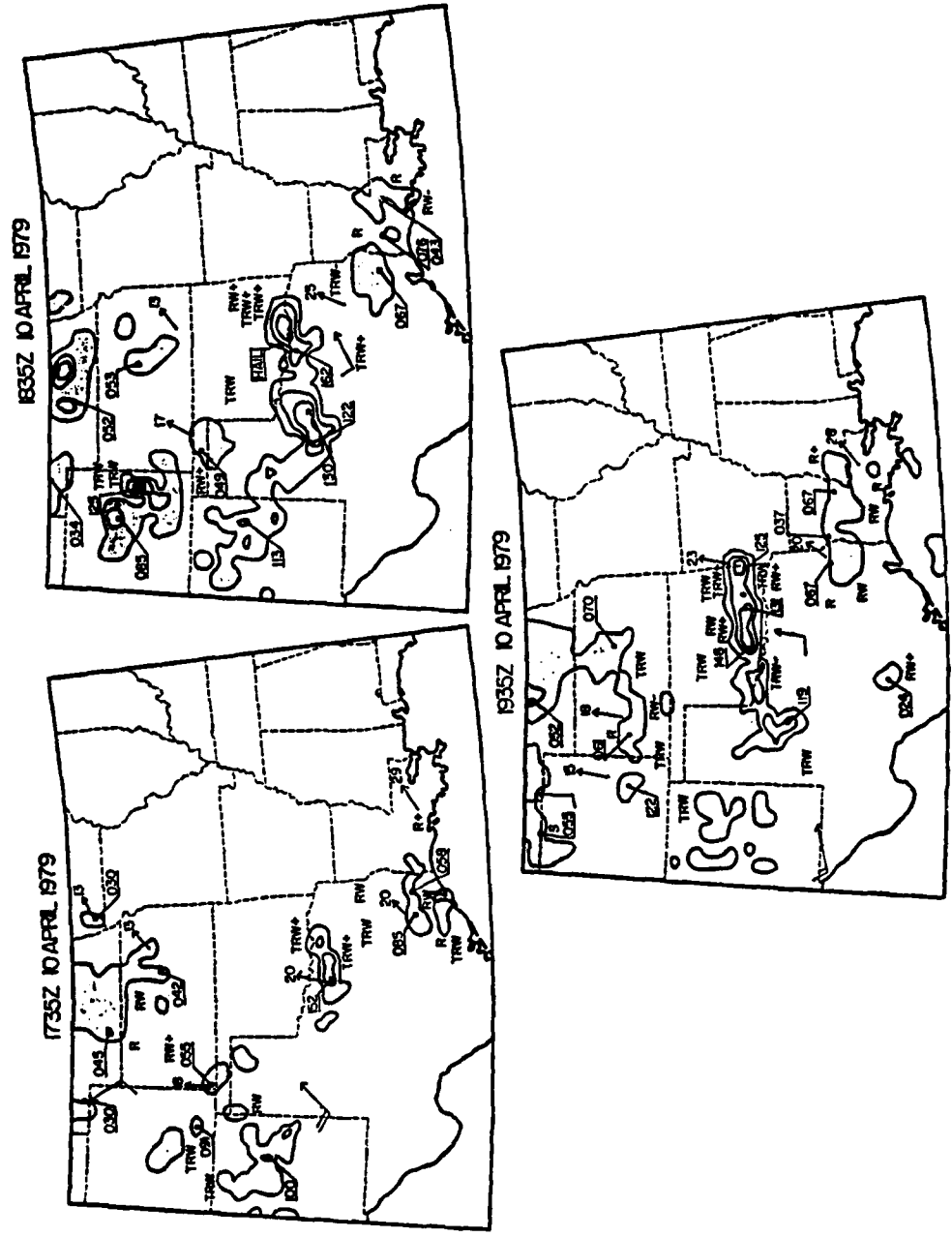
Figure 4.5.

echoes in eastern Texas and western Louisiana which are not reflected in the observed precipitation summary. Unfortunately, the failures of the radar and observed precipitation summaries to match do not follow a systematic pattern. Therefore, it will be necessary to note the specific impacts of these data differences as they become apparent in the qualitiative comparisons of the LHR fields. Despite these differences, it is hoped that taken together these data forms can yield useful insight into the quality of the BLHR calculations, as well as the impact of the three modification schemes.

4.1.1 1200GMT April 10,1979

The BLHR field at this time (Fig.4.1) compares favorably with the other data forms in several areas. The arc of observed precipitation which appears as a broken pattern curving from eastern Colorado through Kansas and Missouri and into Arkansas is generally matched by both the satellite-derived cloud cover and the radar summary. BLHR values also reflect this precipitation pattern even to the extent of pinpointing the observed precipitation maximum in eastern Arkansas. In addition, the BLHR maximum in eastern Texas can be justified by the radar reports near the Louisiana border, although this rapidly moving area of convection is not reflected in the observed precipitation field. Also, observed precipitation in

northcentral Texas extending into Oklahoma is matched by the calculated precipitation values. A noteable failure of the BLHR calculations is apparent in Mississippi where the presence of relatively strong BLHR values is not supported by either the radar or the observed precipitation summaries.

4.1.2 1800GMT April 10,1979

The BLHR calculations at this time (Fig.4.2) indicate a large area of latent heat release extending from New Mexico northeastward through the panhandle of Texas into Kansas and Missouri. Satellite imagery verifys the presence of clouds in this region, and the radar summary shows good agreement. However, the radar echoes are scattered and the tops are not very high, features that perhaps explain the lack of observed precipitation in portions of this region. BLHR calculations perform well in northcentral Texas as they correctly identify an area of deep convection which is shown on the radar summary. The observed precipitation field is also consistent with these results. As previously noted (Fig.4.5), this area of convection grew rapidly in the next two hours expanding in all directions. This perhaps explains why the observed precipitation area extends well into eastern Oklahoma and western Arkansas. The BLHR summary also indicates an area of latent heating in southeastern Texas and Louisiana.

The radar summary is in good agreement, and the satellite depiction also shows extensive cloud cover in this area. However, this region failed to record any precipitation.

The BLHR values in northern Missouri are not reflected in the radar fields, nor by the observed precipitation summary. However, cloud cover is indicated in the satellite depiction. In this case the BLHR calculations were dominated by the SLHR component. Further, stratiform clouds are indicated in the satellite photographs. Thus, this may be an area of non-precipitating stratiform clouds yielding echoes too weak for radar identification.

4.1.3 0000GMT April 11,1979

The BLHR estimates for this time (Fig.4.3) show a large area of latent heating throughout much of the SESAME I grid, with the primary latent heating axis extending from southern Missouri through central Oklahoma and into northcentral Texas. The radar and observed precipitation summaries concur with this. The BLHR calculations also do well in pinpointing the observed precipitation noted in Louisiana by the other summaries. In addition, the absence of observed precipitation in Arkansas and southwestern Texas is similarly depicted in the BLHR field.

The BLHR estimates are less successful in northeastern Texas and southeastern Oklahoma, where calculations suggest latent heating which is not confirmed by any of the other three data forms. The BLHR summary also misses the important region of convection south of the Texas-Oklahoma border near the southwestern corner of Oklahoma. All the other summaries indicate its presence.

4.1.4 0600GMT April 11,1979

At this final map time (Fig.4.4), the primary BLHR region has moved eastward with its orientation continuing along a northeast-southwest axis. Both the radar and the observed precipitation summaries agree that the majority of the precipitation extends from northeast Missouri through eastern Oklahoma to central Texas. The BLHR field captures the northern two-thirds of this area. The observed precipitaion maxima are mirrored by BLHR maxima in northeastern Missouri and northeastern Oklahoma. Also, a secondary area of convection in western Kansas shows up well on all the summaries, as does a region of snow showers in eastern Colorado.

The BLHR field fails at two noteable locations. The first is the severe convection seen in the radar summary in northcentral Texas. The BLHR calculations for this area show no convective component of latent heat release

and very small SLHR values. The second is the BLHR precipitation field in eastern Texas and western Louisiana. The radar summary shows that an important radar report in southwestern Louisiana is missing. Still, both the satellite-derived cloud cover and the observed precipitation summaries show no clouds and no precipitation reports for this area.

4.1.5 Synopsis of horizontal depictions

The overview presented here shows that the BLHR fields are reasonably successful in identifying the major areas of precipitation, particularly after the convection becomes organized. The failure of the parameterzation scheme to compare favorably with the observed precipitation fields in some areas can be attributed to a variety of factors. The first derives from the fact that parameterization schemes are intended to depict grid-scale convective and stable latent heating fields. In fact, the observed precipitation and radar summaries show the precipitation to be largely subgrid-scale through 1800GMT, 10 April. By 2100GMT the synoptic-scale forcing becomes more dominant, yielding more organized precipitation distributions. As a result, the BLHR values are more comparable with observed precipitation values at these later times. The contrast between the comparability of these two fields at the earlier and later times will be

demonstrated more quantitatively in Chapter 6.

A second factor, noted by Fuelberg et al. (1985), suggests that in equating rainfall rates with vertically integrated latent heat release values one includes condensation from non-precipitating clouds as well as precipitating clouds that are less than 100% efficient at converting moisture convergence into rainfall. A final factor, noted by Edmon and Vincent(1976), is the time lag that could exist between the occurrence of moisture convergence and the occurrence of precipitation. In deep convection, precipitation may occur downstream from the primary latent heat release region. This time lag was especially prevalent at 1800GMT. Fig.4.2 clearly shows a large area of latent heat release in northcentral Texas with the observed precipitation field extending well into western Arkansas. The wind direction indicated on the radar summary shows that the observed precipitation region is downwind of the area of BLHR values.

4.2. Vertical cross-sections

A significant aspect of the latent heat release is its vertical distribution, presented here as time/height cross-sections of CLHR (Fig.4.6) and SLHR (Fig.4.9). Unfortunately, there is no way to determine the vertical distribution of latent heating from observed precipitation

and radar summaries; thus, the latter are of little value as comparative parameters. Instead, the vertical distributions of latent heat release for the present study are compared to those from two other studies, the vertical profiles of area-averaged heating rates by Fuelberg et al.(1985) and time/height cross-sections by Robertson(1983). In all cases the quantities are area averaged over the entire computational domain.

4.2.1 Vertical distributions of CLHR

The rapid increase in convective activity during the period under consideration is readily seen in the radar summaries presented in Figs.4.1-4.4. This increased convection is also indicated by the marked increase in CLHR that took place after 1500GMT 10 April (Fig.4.6). The maximum CLHR occurred in the 400 mb-500 mb layer at 0000GMT.

When these cross-sections are compared with the vertical profiles of Fuelberg et al. (1985)(Fig.4.7), generally good agreement is seen. Both distributions indicate increasing CLHR through 0000GMT 11 April and then decreasing at 0600GMT, with the weakest CLHR occurring at 1200GMT and the strongest at 0000GMT. This was true at nearly every pressure level. Also, Fuelberg's vertical profiles agree that the maximum CLHR values occurred in
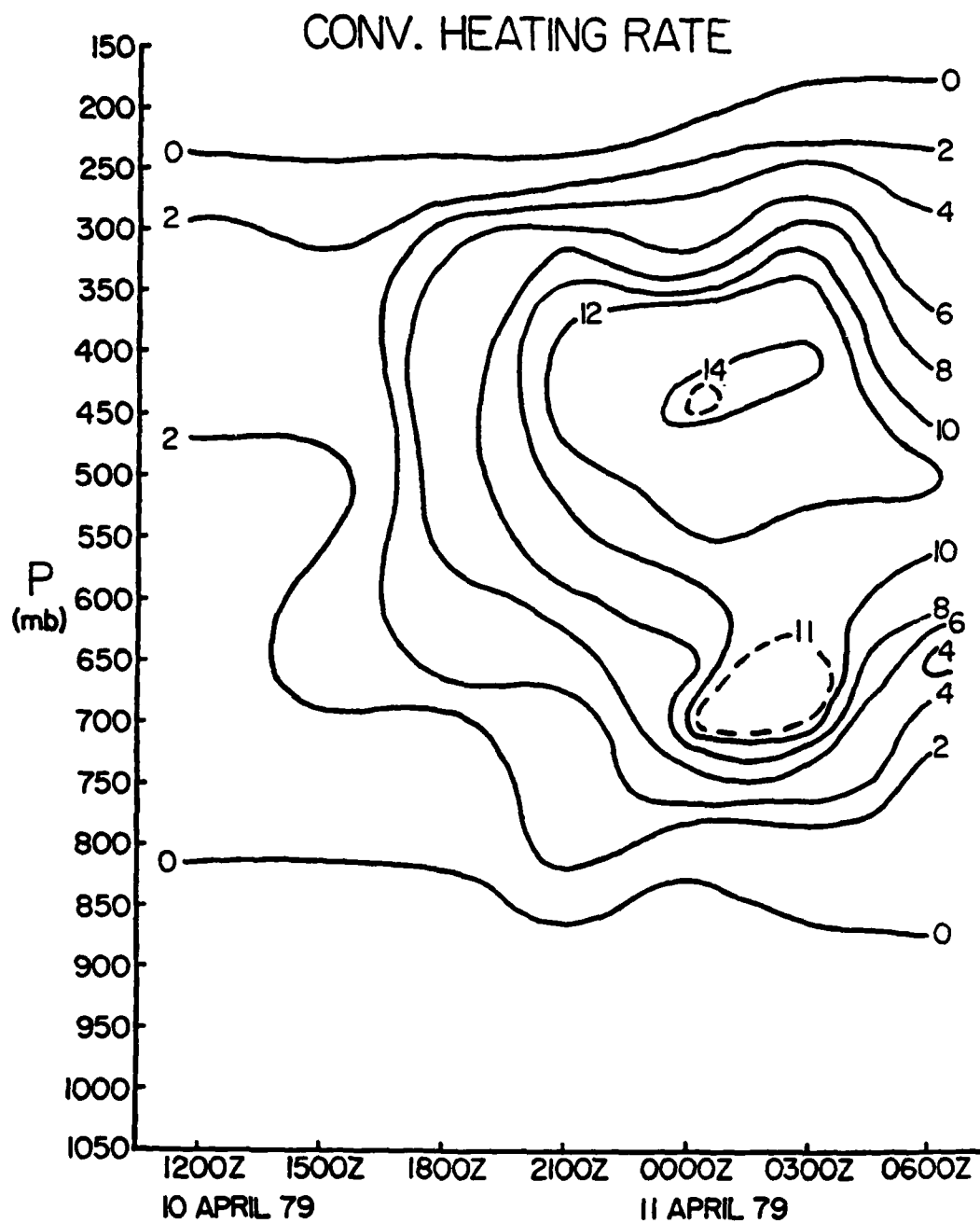
Figure 4.6. Time/height cross-section of BLHR convective component(deg day^{-1}).
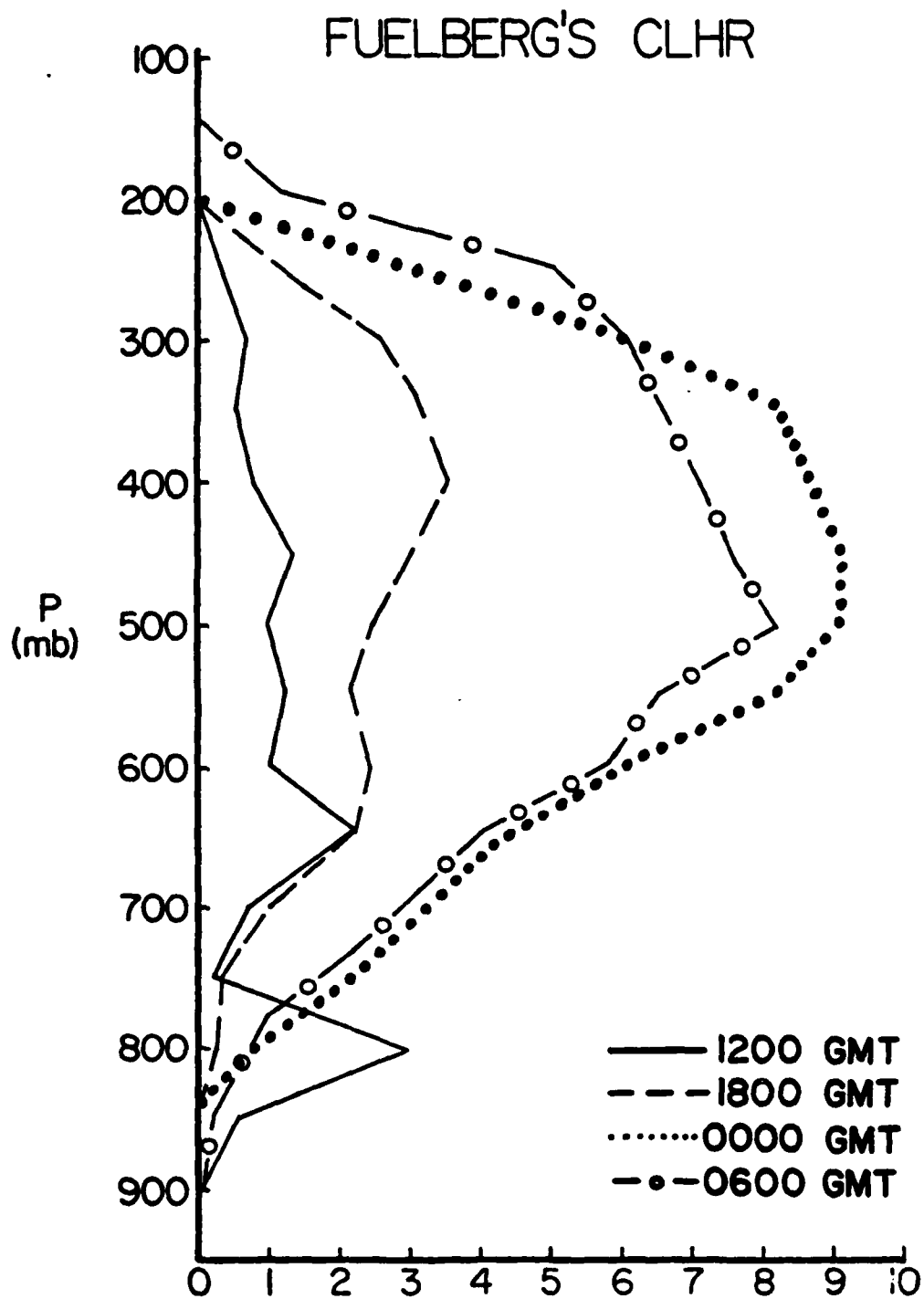
FUELBERG'S CLHR

Figure 4.7. Vertical profiles of convective LHR from Fuelberg et al. (1985)(deg day^{-1}).

the 400-500 mb layer for the latter three time periods and that the bulk of the CLHR took place between 800 mb and 200 mb. Similarities in the two sets of results are not surprising since Fuelberg's computational schemes were similar to those used in this study. Differences that are apparent in the two sets of results can be attributed to Fuelberg's use of a different data analysis procedure, a somewhat larger grid spacing, and slightly different modifications of the basic parameterization scheme. In particular, it should be noted that most of Fuelberg's values ranged from $2-8^\circ Cday^{-1}$, while the results of this study were a factor of two higher.

A CLHR vertical cross section was also obtained from the work done by Robertson(1983)(Fig.4.8). In his study, the grid-scale heating from convection was derived using a mass flux technique which incorporated a 1-D cloud model and includes consideration of precipitation observed at the ground and the cloud structure observed from SMS-I/ GOES IR imagery. Since Robertson's scheme does not depend on the Kuo parameterization, it yields much more independent comparative statistics than does the Fuelberg et al. (1985) paper. In general, Robertson's results contain the same characteristics found in the vertical CLHR distributions of this study. However, Robertson's area-averaged CLHR values were, on the whole, a factor of two smaller than those calculated in this study.

ROBERTSON'S CONV. HEATING RATE
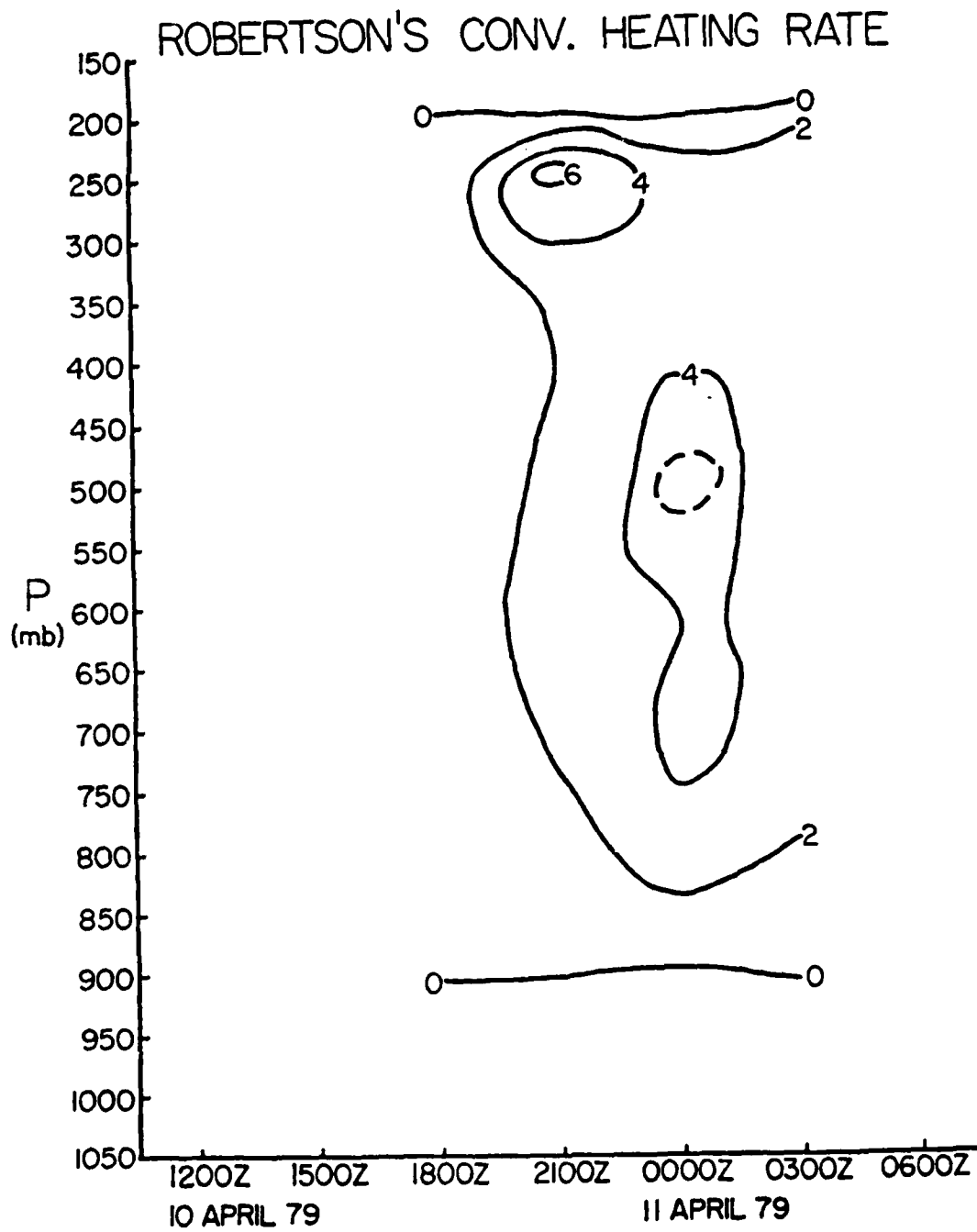
Figure 4.8. Vertical cross-section of convective LHR from Robertson(1983)(deg day^{-1}).

4.2.2 Vertical distributions of SLHR

The SLHR vertical distributions(Fig.4.9) also show an increase throughout the period of this study. This is in response to an increased flow of moist air from the Gulf of Mexico over the eastern two-thirds of the area. This, coupled with an expanding area of upward motion (Moore and Fuelberg, 1981), supports the larger SLHR values found late in the period. When compared with the Fuelberg et al. (1985) vertical profiles(Fig.4.10), both show a general increase of SLHR values at nearly all levels throughout the period. However, as with the CLHR results, the SLHR values in this study are on the whole larger than those found in Fuelberg. The variations mentioned earlier (see section 4.2), as well as his use of 90% relative humidity as a discriminator for SLHR calculations (compared to the 80% used in this study), can be identified as reasons for differences seen in the two sets of results.
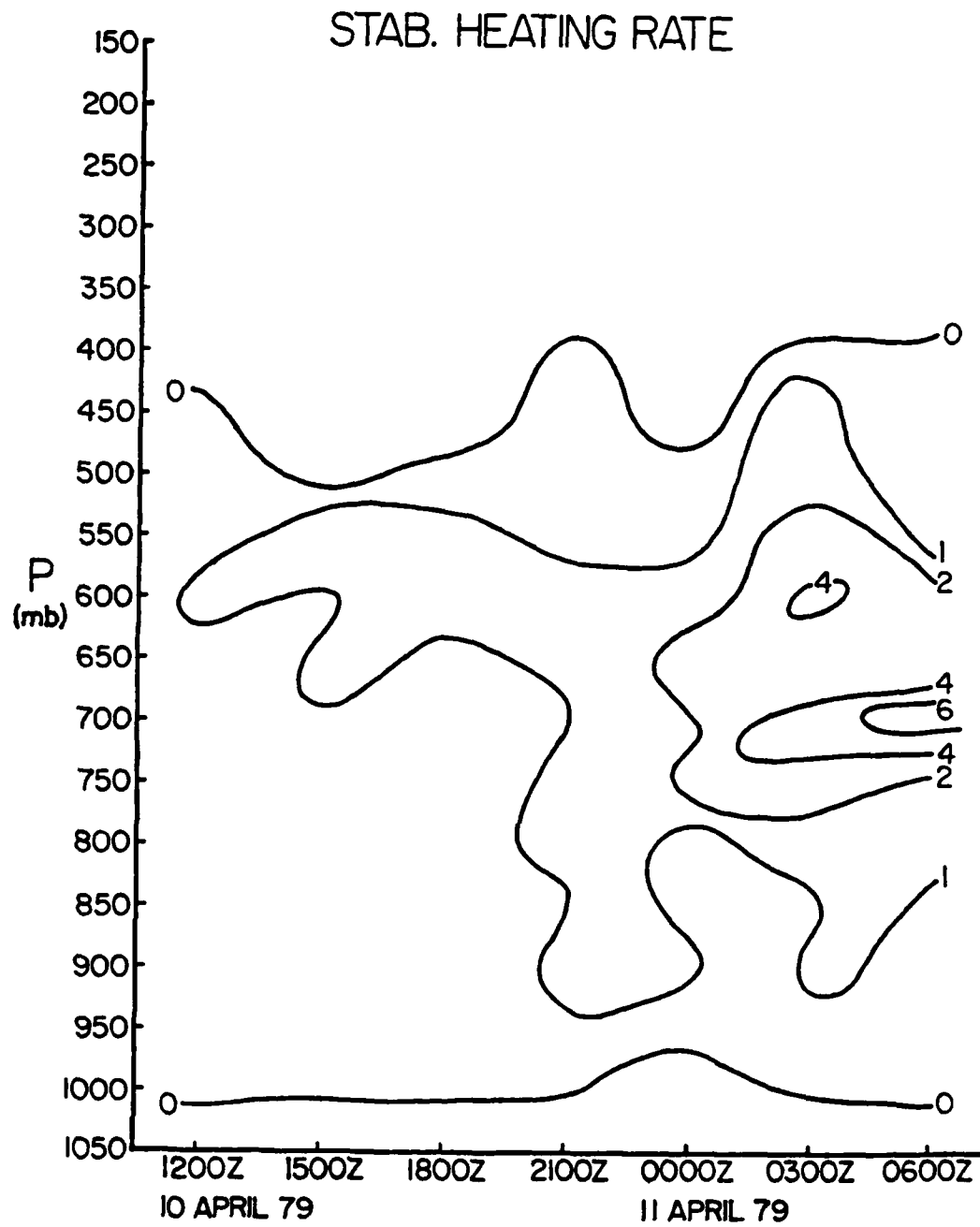
Figure 4.9. Vertical cross-section BLHR stable component (deg day^{-1}).

FUELBERG'S SLHR
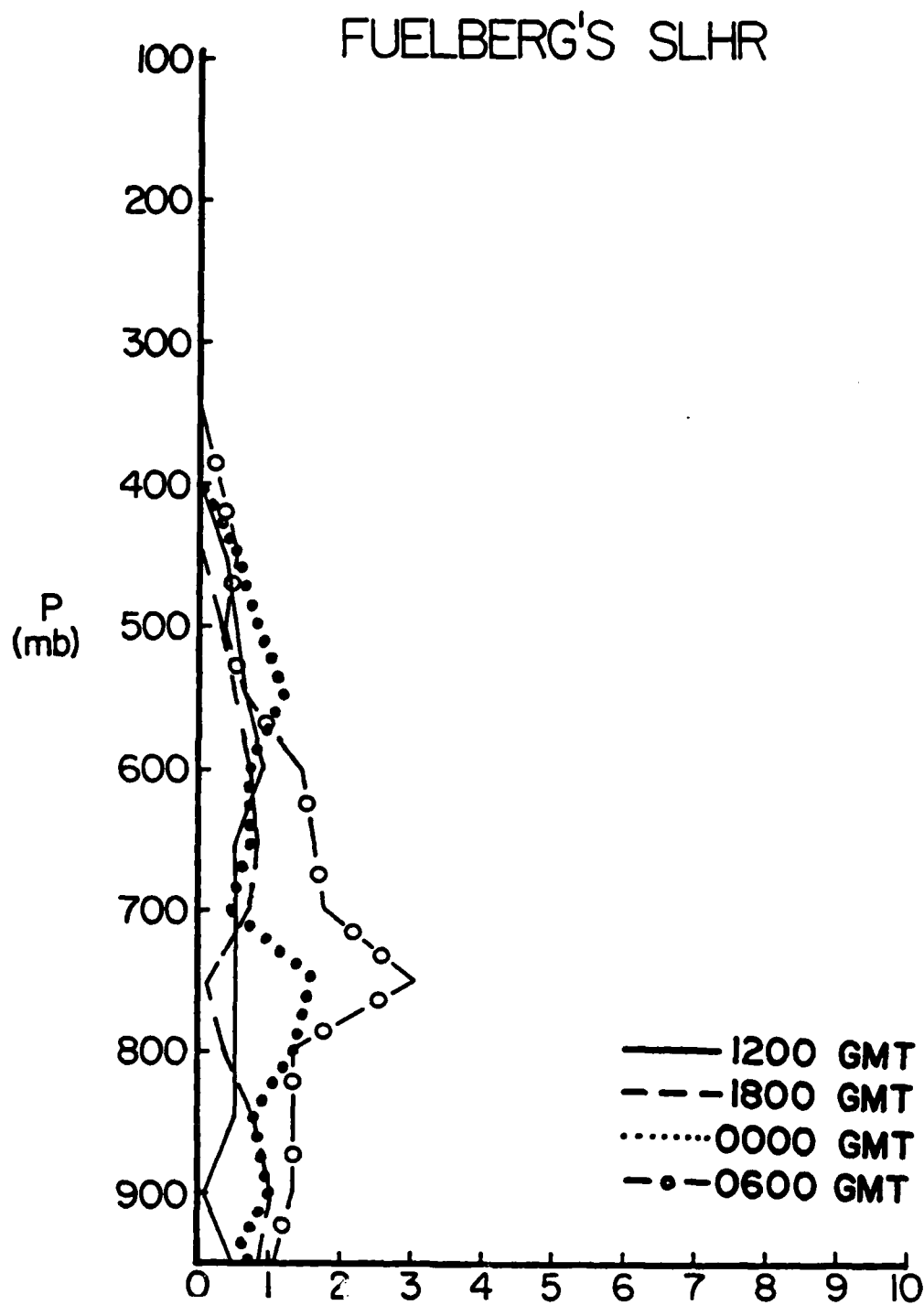
Figure 4.10. Vertical profiles of stable LHR from Fuelberg et al.(1985)(deg day^{-1}).

5. THE MODIFIED LATENT HEAT RELEASE CALCULATIONS

5.1 Horizontal distributions

This chapter presents an analysis of the changes in the latent heat release fields brought about by the three modification schemes summarized in chapter 2. As in the preceding chapter comparisons are made between the modified latent heat release fields(MLHR1,2,3),radar patterns, and observed precipitation summaries. These fields and the previously discussed BLHR values are presented in Figs.5.1-5.4.

5.1.1 1200GMT April 10, 1979

The unenhanced satellite cloud image(Fig.4.1) for this time results in the retention of the arc of BLHR values(Fig.5.1) that extends from eastern Colorado eastward through Kansas and Missouri and then southward through Arkansas. This area, which is also reflected in the observed precipitation and radar summaries, is presented as nearly continuous in the MLHR1 and MLHR3 fields. The MLHR2 modification presents a much more broken pattern depiction, which matches more closely the

54

Figure 5.1. Top left: NMC radar summary chart for 1200GMT
10 April 1979. Cloud tops in dam, motion
vectors in m s^{-1}.
Top right: Observed precipitation rate(mm h^{-1})
for 1200GMT 10 April 1979.
Middle left: Vertically integrated BLHR
combining convective and stable components(mm
h^{-1}).
Middle right: Vertically integrated MLHR1
combining convective and stable components(mm
h^{-1}).
Bottom left: Vertically integrated MLHR2
combining convective and stable components(mm
h^{-1}).
Bottom right: Vertically integrated MLHR3
combining convective and stable components(mm
h^{-1}).
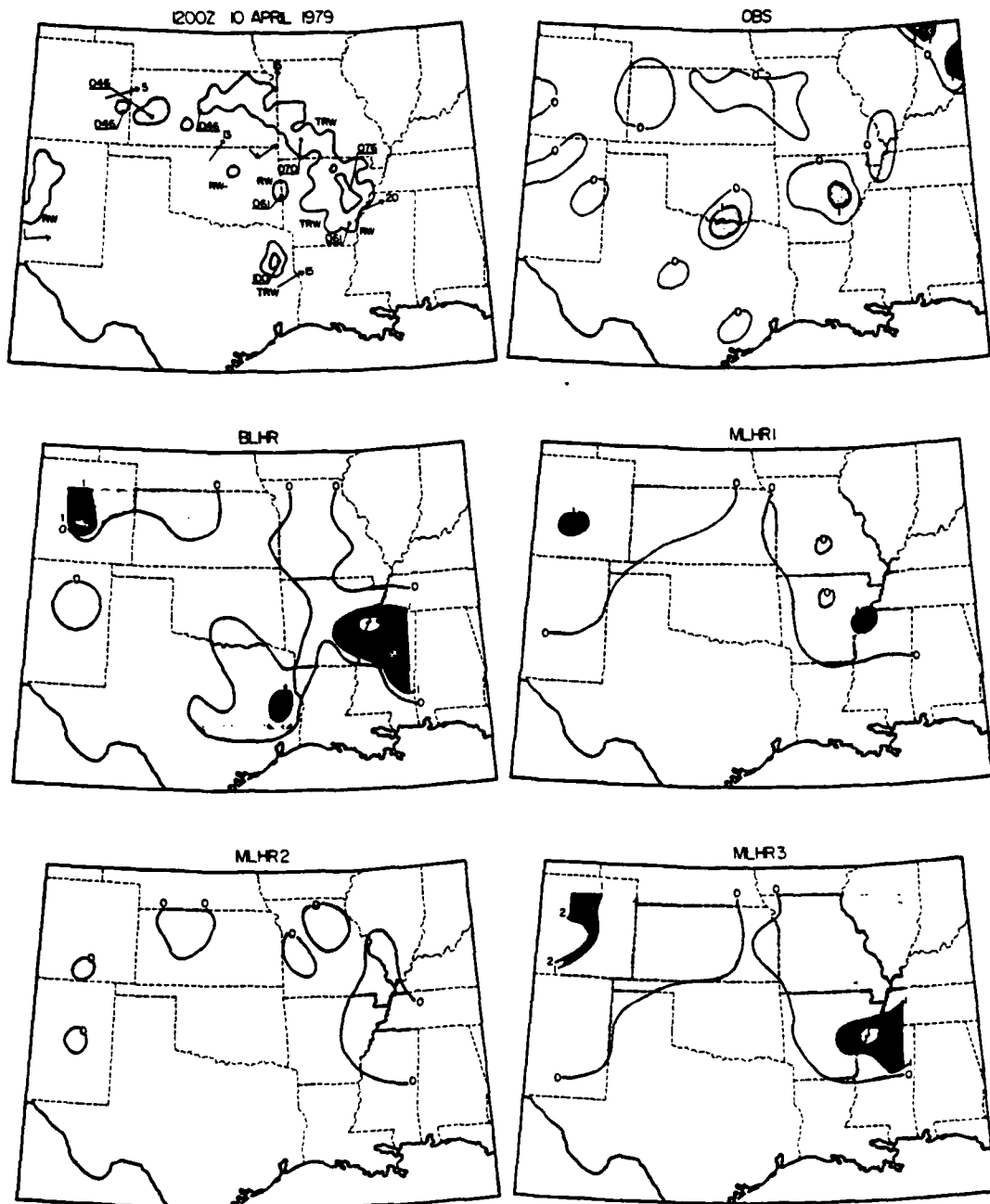
Figure 5.1.

Figure 5.2. Top left: NMC radar summary chart for 1800GMT
10 April 1979. Cloud tops in dam, motion
vectors in m s^{-1}.
Top right: Observed precipitation rate(mm h^{-1})
for 1800GMT 10 April 1979.
Middle left: Vertically integrated BLHR
combining convective and stable components(mm
h^{-1}).
Middle right: Vertically integrated MLHR1
combining convective and stable components(mm
h^{-1}).
Bottom left: Vertically integrated MLHR2
combining convective and stable components(mm
h^{-1}).
Bottom right: Vertically integrated MLHR3
combining convective and stable components(mm
h^{-1}).

1800Z 10 APRIL 1979   OBS

BLHR   MLHR1

MLHR2   MLHR3
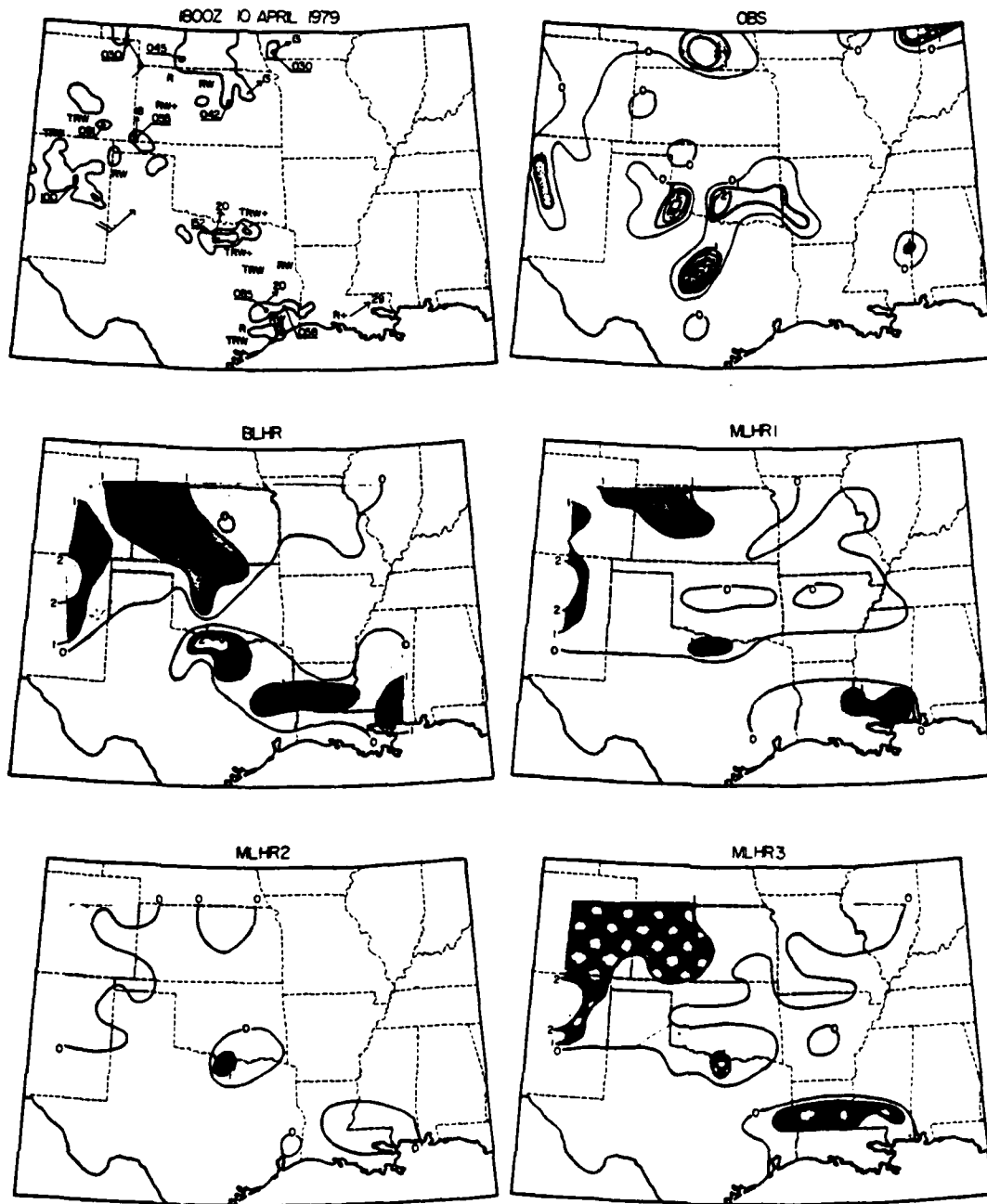
Figure 5.2.

Figure 5.3. Top left: NMC radar summary chart for 0000GMT
11 April 1979. Cloud tops in dam, motion
vectors in m s^{-1}.
Top right: Observed precipitation rate(mm h^{-1})
for 0000GMT 11 April 1979.
Middle left: Vertically integrated BLHR
combining convective and stable components(mm
h^{-1}).
Middle right: Vertically integrated MLHR1
combining convective and stable components(mm
h^{-1}).
Bottom left: Vertically integrated MLHR2
combining convective and stable components(mm
h^{-1}).
Bottom right: Vertically integrated MLHR3
combining convective and stable components((mm
h^{-1}).
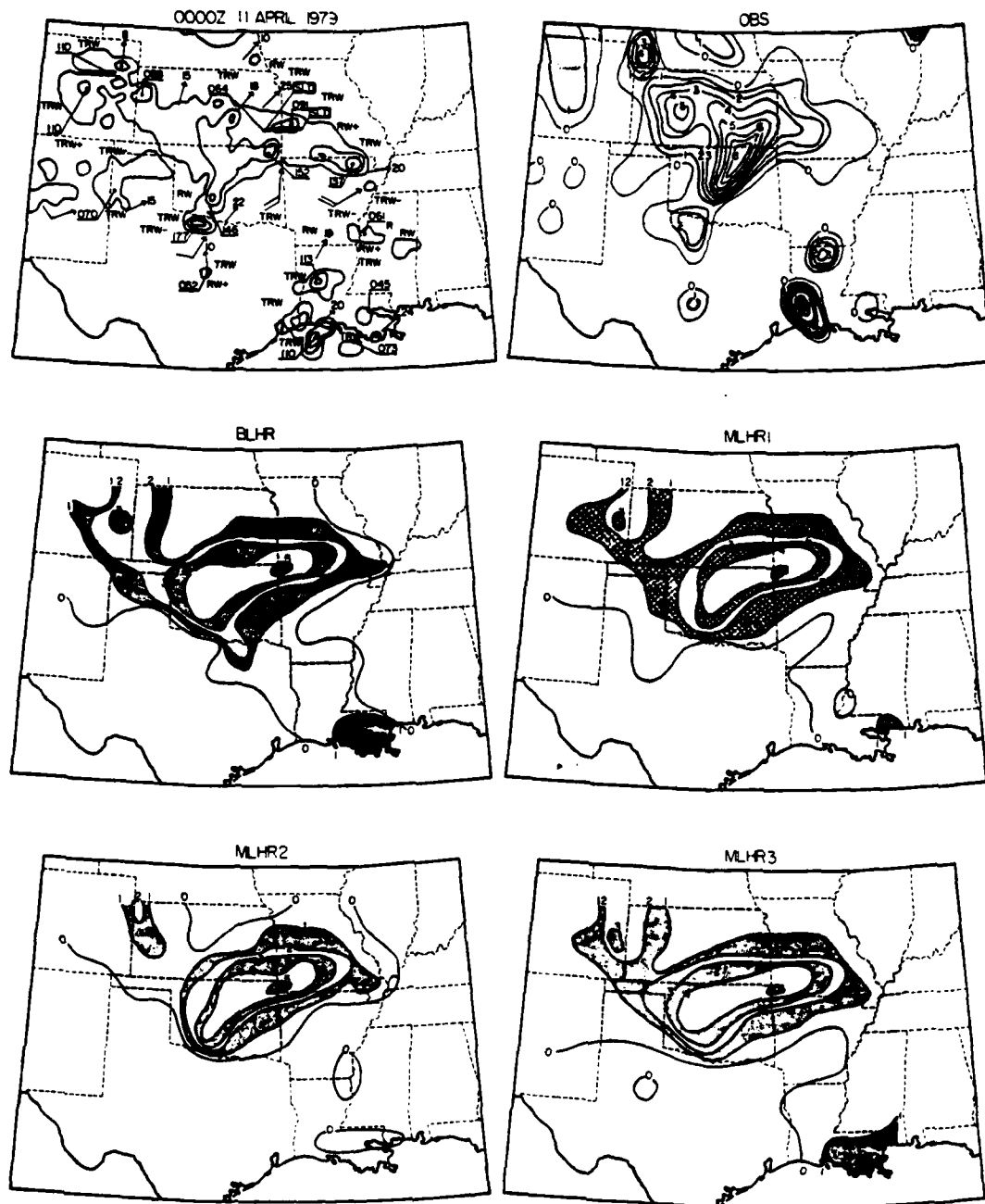
Figure 5.3.

Figure 5.4. Top left: NMC radar summary chart for 0600GMT
11 April 1979. Cloud tops in dam, motion
vectors in m s^{-1}.
Top right: Observed precipitation rate(mm h^{-1})
for 0600GMT 11 April 1979.
Middle left: Vertically integrated BLHR
combining convective and stable components(mm
h^{-1}).
Middle right: Vertically integrated MLHR1
combining convective and stable components(mm
h^{-1}).
Bottom left: Vertically integrated MLHR2
combining convective and stable components(mm
h^{-1}).
Bottom right: Vertically integrated MLHR3
combining convective and stable components(mm
h^{-1}).
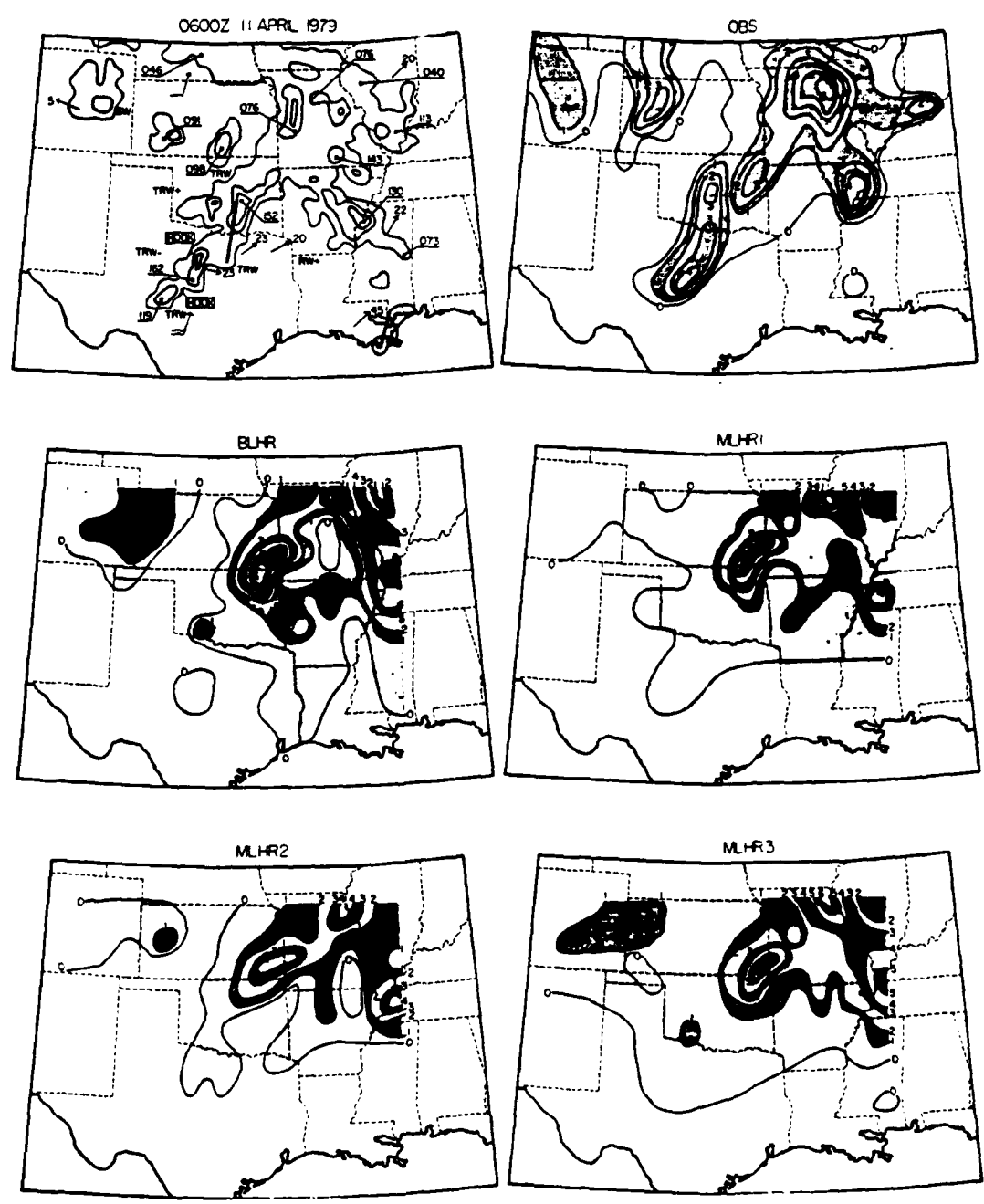
Figure 5.4.

general characteristics of the observed precipitation
pattern. A similar result is seen over New Mexico, where
the MLHR1 and MLHR3 schemes increase the areal coverage of
calculated latent heat release. The MLHR2 pattern again
suggests spotty latent heating, in general agreement with
both the observed precipitation and radar fields.

5.1.2 1800GMT April 10, 1979

The principle region of latent heat release extending
from New Mexico northward through Colorado and southern
Nebraska is preserved by all three modifications, although
it is perhaps too small in the MLHR2 depiction, Further, a
small latent heat release area in southern Louisiana is
identified in all of the modifications. This feature is
supported by the radar summary but is not depicted in the
observed precipitation summary.

The most striking differences are seen in northern
Texas, Oklahoma, Arkansas, and Missouri. Both the MLHR1
and MLHR3 modifications show extensive latent heating in
these areas, much of which is unsupported either by the
radar or the observed precipitation summaries. The MLHR2
field presents a much more satisfactory pattern, although
it clearly underestimates the extent of the observed
precipitation in northern Texas and Oklahoma. All of the
modifications fail to extend latent heating values into

central Texas to account for the precipitation that is indicated by the observed precipitation summary.

5.1.3 0000GMT April 11, 1979

An extensive precipitation pattern depicted by both the radar and the observed precipitation summaries extends from northern Texas through Oklahoma into Kansas, and then eastward into Missouri and Arkansas. All modifications reflect this region very well, even to the extent of identifying the axis of heaviest precipitation which extends from southern Missouri through central Oklahoma and into northcentral Texas. Both the MLHR1 and MLHR3 modifications indicate latent heat release in Louisiana, separating this area from the larger precipitation region to the north. The MLHR2 pattern also eliminates latent heating in eastern Texas and southwestern Arkansas, but its Louisiana values are not as well placed as the other modifications.

5.1.4 0600GMT April 11, 1979

Once again, all of the modifications mirror the large precipitation area, including the maximum precipitation axis extending from northeastern Missouri through eastern Oklahoma and into central Texas. The modifications are able to pinpoint the northern two precipitation maxima,

one in northeastern Missouri and the other in northeastern Oklahoma, and also reflect the relatively unbroken nature of this axis as it extends into central Texas. This pattern appears to be more reasonable than the broken pattern of latent heat release suggested by the BLHR field. In addition, the MLHR1 and MLHR3 modifications in this area extend values further south into Texas than is seen in the BLHR and MLHR2 calculations, and all three modifications successfully eliminate BLHR values calculated in eastern Texas and western Louisiana. Finally, contrary to the other two modifications, the MLHR3 field extends into the Texas panhandle and northern New Mexico, a feature that is not reflected by the radar and observed precipitation summaries.

5.1.5 Synopsis of horizontal depictions

In evaluating the various modifications made to the BLHR calculations, some important points become readily apparent. In cases where the BLHR calculations did very poorly in reflecting observed precipitation, the modifications were able to make some dramatic changes in the areal coverage of the calculated precipitation fields. This was found to be true especially early in the study period. After 2100GMT, the BLHR calculations were much more successful in identifying the pattern of observed precipitation. At these later times the modifications

made changes in some areas, but the overall latent heating pattern remained relatively unaffected. It can also be seen that neither the BLHR calculations nor the modifications succeeded in capturing isolated convective activity well. This isolated convection was most prevalent in the two early time periods of 1200GMT and 1800GMT.

It is premature at this point to advance one modification as superior to the others or to state conclusively that any of them are more precise than the BLHR calculations. Yet several important observations can be made concerning the different modifications used in this study. The calculated precipitation fields produced by the 235K enhancement modification (MLHR2) consistently matched the radar summary much closer than the fields of the other modifications. This supports the contention made in a study done by Arkin(1979) that the 235K threshold is able to isolate the regions of convective precipitation occurring in a cloud field. However, the MLHR2 modification also failed to identify some areas of light precipitation which were captured by the raingauge network. While the 235K enhancement reduced the latent heating estimate by decreasing the areal coverage of latent heat release, the 3-layer enhancement(MLHR3) typically increased the areal coverage of calculated latent heating. This was accomplished by producing values

at points that were missed in the BLHR calculations, but where there was cloud cover. While under certain circumstances this caused the calculated precipitation patterns to better reflect the radar and observed precipitation summaries, improvement was not always noted. Frequently, this third modification returned latent heat release values to regions which had been vacated by the main precipitation area, but in which cloud cover lingered behind. Finally, the MLHR1 and MLHR3 modifications calculated latent heat release in regions that were influenced by the cloud cover preceding and surrounding a major precipitation region. This tendency for the calculated latent heat release fields to envelope the observed precipitation fields matches some of the conclusions found in the work done by Lin and Smith(1985) and may reflect the ability of the computational schemes to identify latent heat release in non-precipitating regions.

5.2 Vertical cross-sections

The modifications used in this study affect the vertical distribution of th' BLHR values in different ways. As described in Chapter 2, the MLHR1 and MLHR3 modifications impact the total BLHR values, while the MLHR2 scheme modifies the two components of latent heat release separately. Therefore, a complete evaluation of

the vertical latent heat release distributions is limited to the TLHR values for both the basic and modified calculations. These in turn can be compared with vertical profiles of the sum of the two components of LHR presented by Fuelberg et al. (1985) (see section 4.2).

Vertical cross-sections of BLHR, MLHR1, MLHR2, and MLHR3 are presented in Fig.5.5. Several important points are immediately apparent. This figure shows that the basic pattern of BLHR values remains relatively unaltered by the modifications. All cross-sections show latent heat release increasing at virtually all levels prior to 0300GMT, with the bulk of LHR occurring between 750 mb and 350 mb. Also, each modification reflects the double maxima seen near 700 mb and 400 mb at 0300GMT in the BLHR calculation.

The greatest impact from the modifications is on the magnitudes of the latent heat release values. The MLHR2, and to a lesser extent the MLHR1 scheme, reduces the area-averaged total latent heat release values at nearly every time and level, while the MLHR3 modification retains nearly the same magnitudes. These conclusions are similar to the observations presented in the evaluation of the horizontal LHR fields; that is, the MLHR2 modification has the largest impact on the BLHR values, and, in fact, reduces the latent heating estimates. Also, while the MLHR3 modification succeeds in eliminating LHR values at

Figure 5.5. Top left: Vertical cross-section of BLHR combining convective and stable components(deg day^{-1}).
Top right: Vertical cross-section of MLHR1 combining convective and stable components(deg day^{-1}).
Bottom left: Vertical cross-section of MLHR2 combining convective and stable components(deg day^{-1}).
Bottom right: Vertical cross-section of MLHR3 combining convective and stable components(deg day^{-1}).
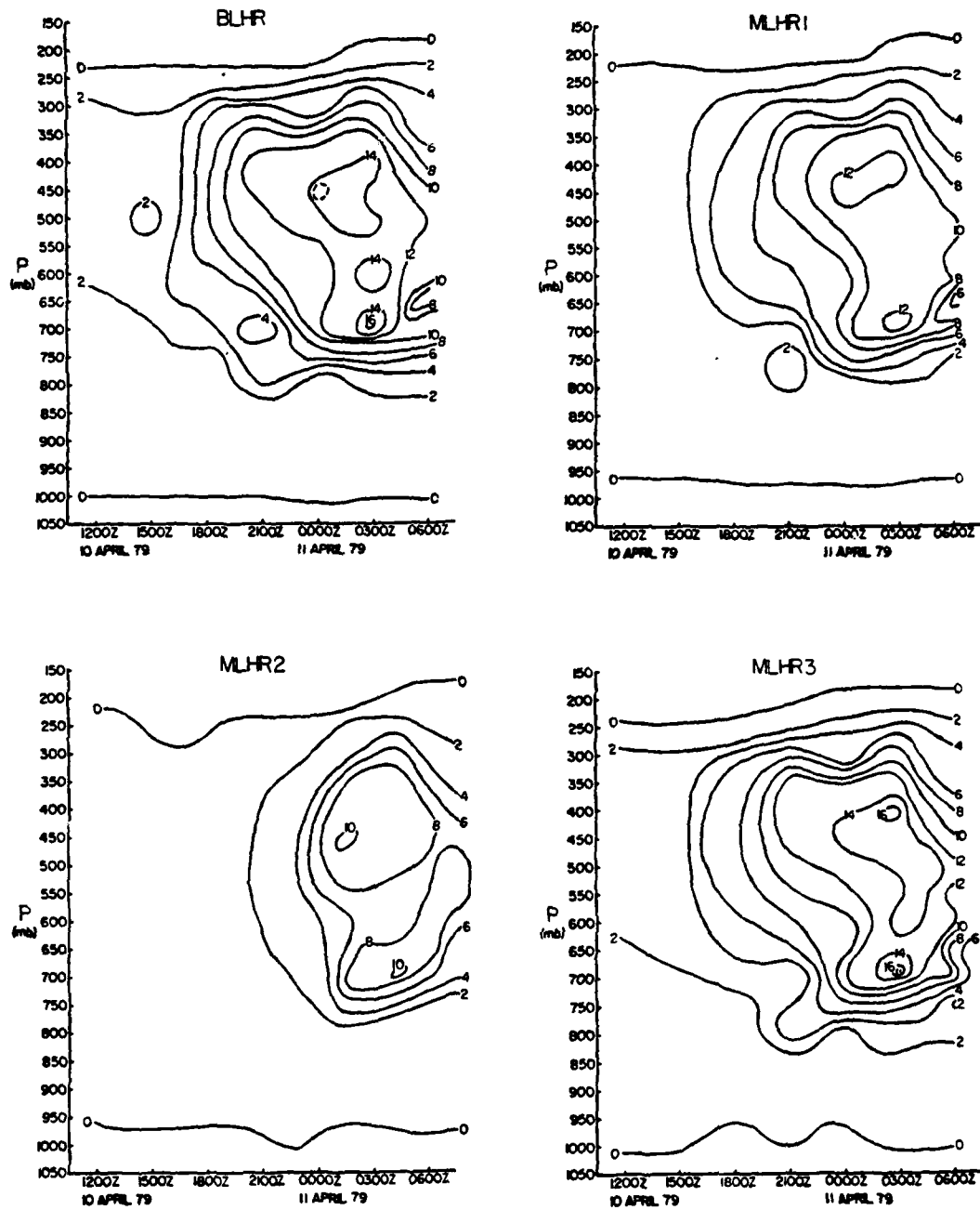
Figure 5.5.

some grid points and at various levels in the vertical, this modification also returns values at other points and levels, thus leaving the overall average values relatively unaffected.

The vertical profiles of the two components of LHR provided in the study of Fuelberg et al. (1985) were summed at each pressure level in order to obtain a vertical distribution of TLHR. The resulting profile is shown in Fig.5.6. Fuelberg provided values for only four time periods that were common with the times used in this study. Fuelberg's calculations indicate that the maximum latent heating takes place between 0000GMT and 0600GMT, in good agreement with this study's results. Both distributions have the bulk of the LHR occurring between 700 mb and 350 mb. For the latter three time periods Fuelberg indicated that the maximum LHR occurred between 400 mb and 550 mb, also in agreement with this study's findings. Of the three modifications, the MLHR2 vertical cross-section provides LHR values that are closer in magnitude to Fuelberg's results. Differences in the vertical distributions of LHR found in the modified calculations and those of Fuelberg are similar to those found in the BLHR estimates.

Finally, since the MLHR2 results are the most comparable with the Fuelberg et al. (1985) profiles, it is of interest to compare the convective component of these

FUELBERG'S TLHR
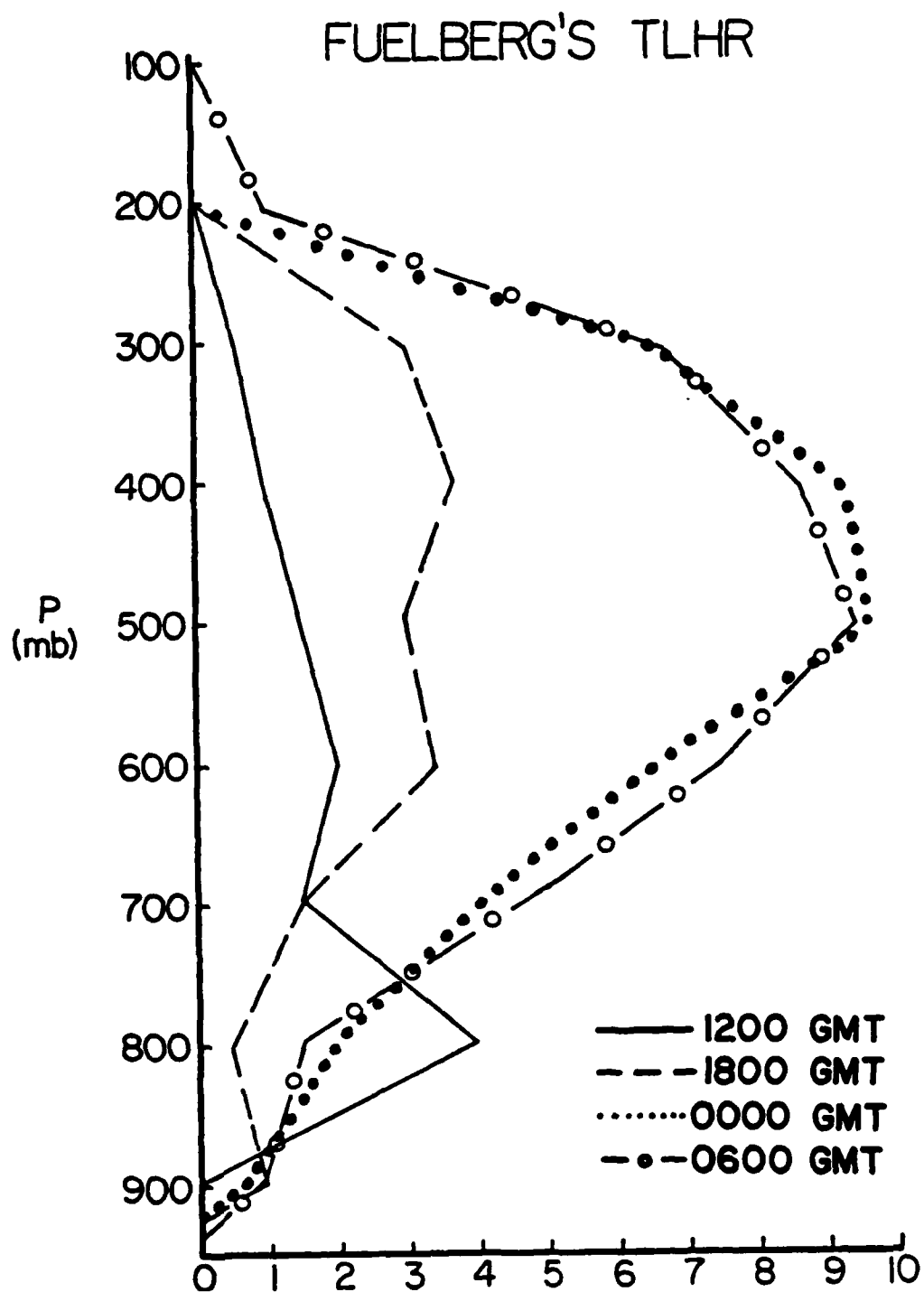
Figure 5.6. Vertical profiles of LHR combining convective and stable components from Fuelberg et al. (1985)(deg day^{-1}).

Legend:
—— 1200 GMT
– – – 1800 GMT
········· 0000 GMT
–•– 0600 GMT

P (mb) axis values: 100, 200, 300, 400, 500, 600, 700, 800, 900

Horizontal axis values: 0 1 2 3 4 5 6 7 8 9 10

results with those of Robertson(1983), discussed in section 4.2. Fig.5.7 shows the cross-sections of the MLHR2 convective component together with that of Robertson. Comparing this with the BLHR convective component displayed in Fig.4.6, it is clear that, although still larger, the MLHR2 values are significantly closer to the Robertson's results than are the basic convective latent heating values.
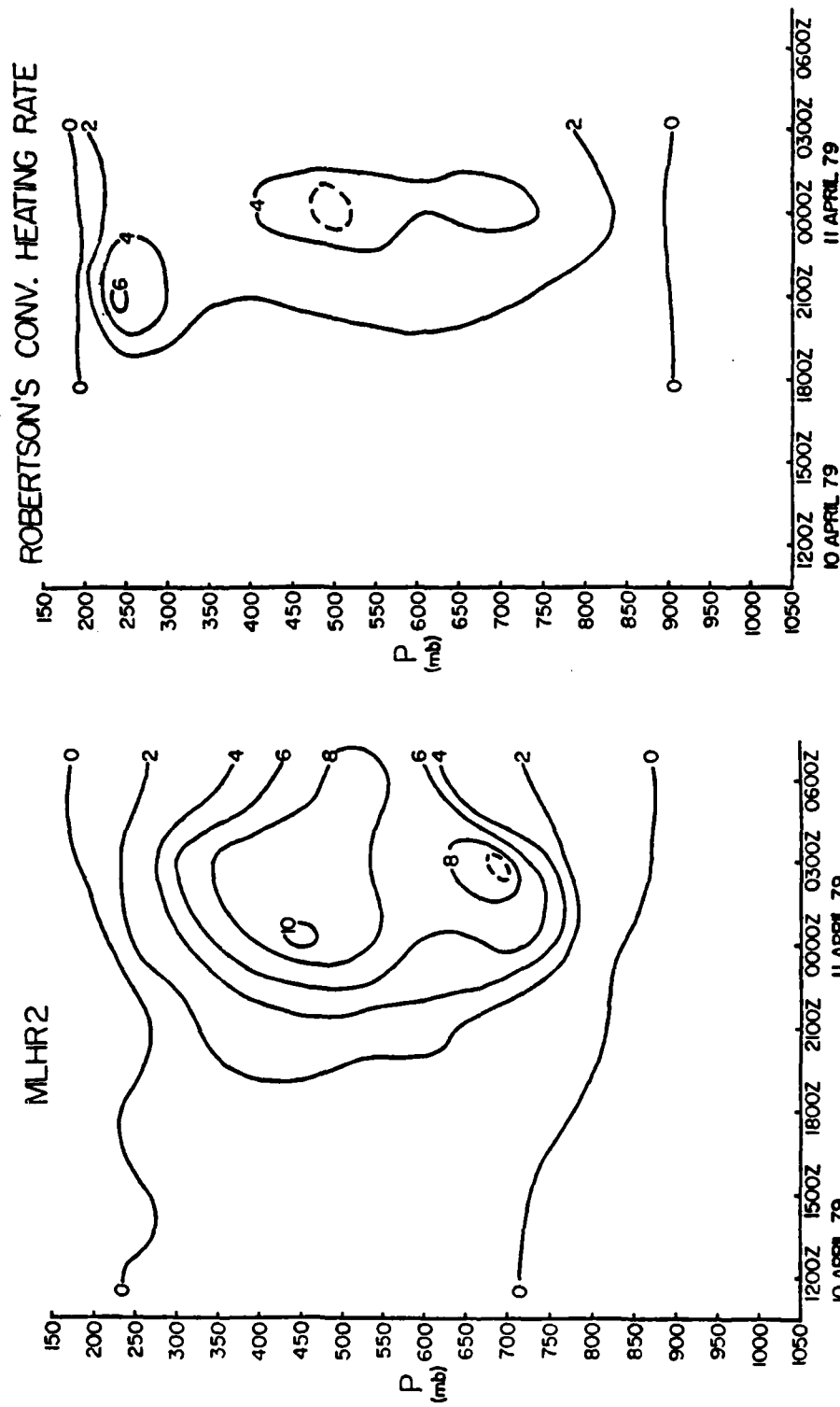
Figure 5.7. Left: Vertical cross-section of MLHR2
convective LHR(deg day⁻¹).
Right: Vertical cross-section of convective
LHR from Robertson(1983)(deg day⁻¹).

6. FURTHER EVALUATION OF BASIC AND MODIFIED LHR CALCULATIONS

6.1 Area-averaged values

Despite the shortcomings mentioned in section 4.1 concerning the use of gridded precipitation totals, these values remain the most independent standard available for an evaluation of LHR calculations. This evaluation serves to compliment the conclusions drawn earlier in the qualitative comparison of horizontal and vertical LHR distributions. The simplest and least detailed statistics which can be considered in this evaluation are the area-averaged observed precipitation and the basic and modified latent heating values, summarized in Fig.6.1. This figure supports the earlier qualitative observation that precipitation rates increased over the SESAME I grid from 1200GMT 10 April to 0300GMT 11 April. The rapid growth of convection that was depicted in the radar summaries of Fig.4.5 is reflected by the large increase in all of the area-averaged quantities after 1800GMT. This period of large increase corresponds to the time interval during which synoptic-scale forcing became more dominant and more organized precipitation distributions were evident(see
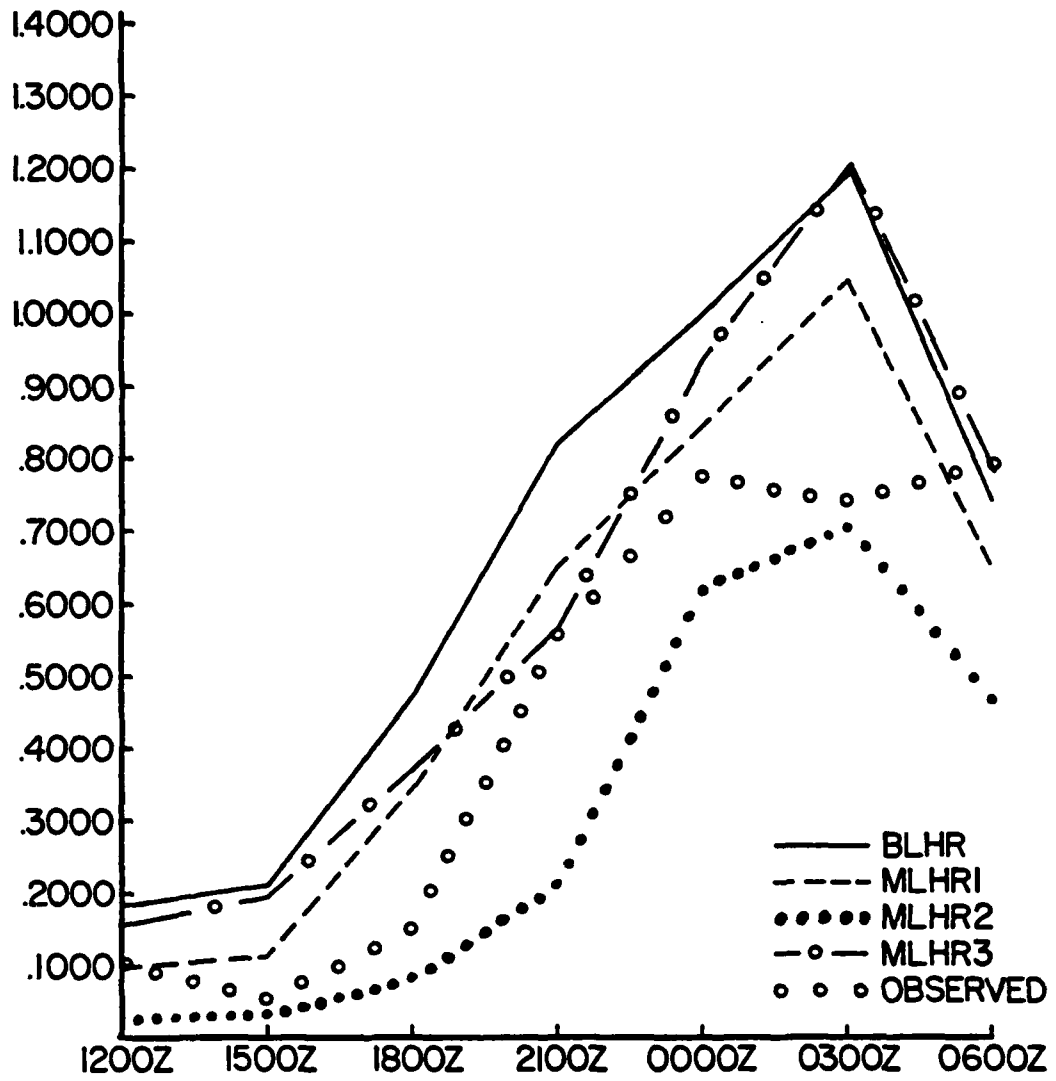
Figure 6.1. Area-averaged observed precipitation and area-averaged basic and modified LHR(mm h^{-1}).

Section 4.1.5). The rapid increase in precipitation amount and its relationship to synoptic-scale forcing suggest that it would be appropriate to summarize these and later statistics by averaging over two periods. Period 1 encompasses the first three map times (1200GMT, 1500GMT, 1800GMT), while Period 2 encompasses the last four map times(2100GMT, 0000GMT, 0300GMT, 0600GMT).

Fig.6.1 shows that, with the exception of 0600GMT, all three modifications reduce the overestimate of latent heating seen in the BLHR totals. The MLHR1 and MLHR3 calculations remain larger, while the MLHR2 are smaller, than the observed precipitation rates. The extent of these modifications is summarized by Table 6.1, which presents the average absolute departures from the area-averaged observed precipitation totals for the basic and modified LHR values. Overall, the MLHR1 modification yields the smallest deviation from the observed area averaged totals; however, in the first period the MLHR2 departure is the smallest. An analysis of variance using an F-test (Hicks,1982) was done on the mean departures of area-averaged basic and modified LHR calculations from the area-averaged observed precipitation values. Using the assumption that an underestimation of area averaged observed precipitation does not hold any advantage over an overestimation, there was found to be no statistical difference between the mean LHR departures, at the 5%

Table 6.1. Departure of area-averaged LHR quantities from area-averaged observed precipitation values.

DEPARTURE FROM OBSERVED

PARAMETER	OVERALL	PERIOD 1	PERIOD 2
BLHR	.21	.19	.24
MLHR1	.12	.09	.15
MLHR2	-.15	-.06	-.21
MLHR3	.15	.14	.16

PERIOD 1   1200GMT - 1800GMT
PERIOD 2   2100GMT - 0600GMT

level of significance. Therefore, these statistics alone offer little to support the superiority of one set of calculations over the others.

6.2 Correlation coefficients

To compare the overall grid point distribution of observed precipitation with those of the basic and modified LHR values, these correlation coefficients were computed and are shown in Fig.6.2. The ability of the various latent heat release calculations to reflect the observed precipitation distribution varies greatly from Period 1 to Period 2. At the first three map times, when the precipitation field was largely subgrid-scale, correlations are very small. After 1800GMT the correlation coefficients rise rapidly for all of the schemes. Fig.6.2 also shows that at every map time all of the modifications have higher correlation coefficients than do the BLHR calculations, with the MLHR2 modification yielding the best correlations.

Table 6.2 summarizes the Fig.6.2 results by focusing on the percentage improvement in the correlation coefficients produced by the modifications. This table again shows that all three modifications improved the BLHR calculations. The relative impact of these modifications is especially noteable in Period 1, although the
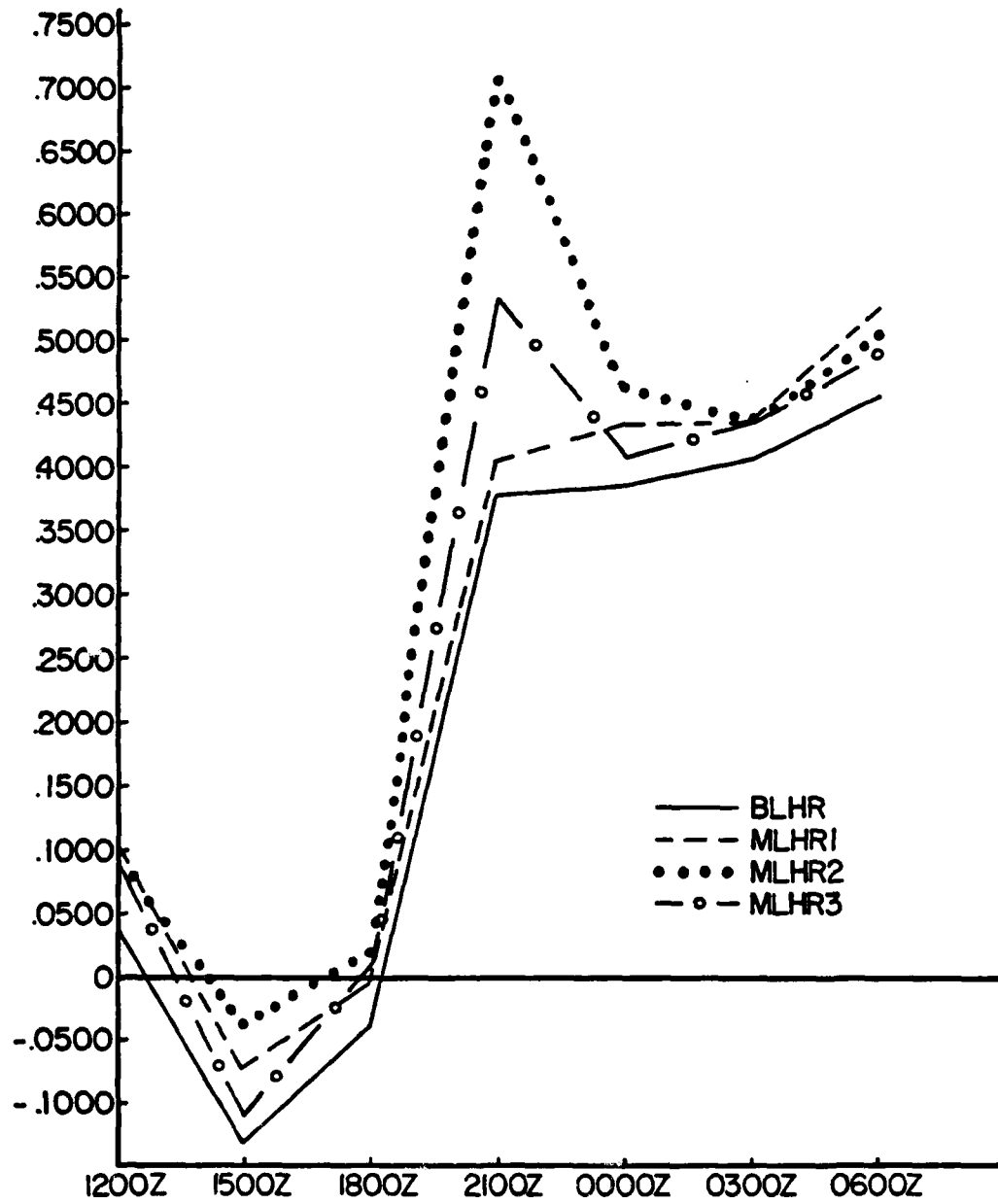
Figure 6.2. Correlation coefficients between
basic and modified LHR
calculations.
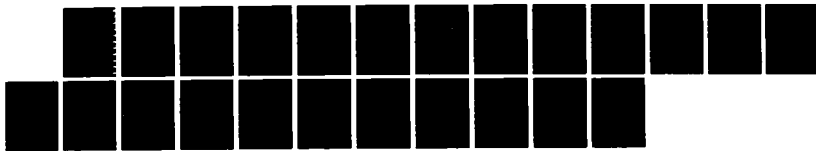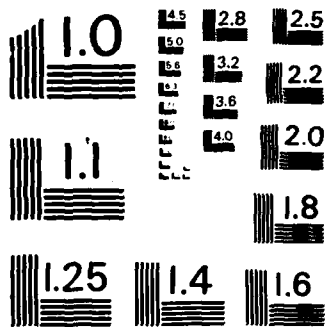
MICROCOPY RESOLUTION TEST CHART

NATIONAL BUREAU OF STANDARDS-1963-A

Table 6.2. Percent improvement of modified over basic LHR
correlation coefficients.

PERCENT IMPROVEMENT
FROM BLHR VALUES

MODIFICATION	OVERALL	PERIOD 1	PERIOD 2
MLHR1	23%	73%	10%
MLHR2	45%	101%	28%
MLHR3	23%	60%	14%

PERIOD 1   1200GMT - 1800GMT
PERIOD 2   2100GMT - 0600GMT

% Improvement = $\dfrac{\text{MOD VALUE} - \text{BLHR}}{\text{BLHR}}$ X 100%

correlations remain very poor. The MLHR2 modification
yields the greatest improvement in both periods. An
analysis of variance using an F-test (Hicks,1982) was done
on the mean correlation coefficients for the basic and the
modified calculations. It was found that there was a
significant variation in these values. A Newman-Kuels
range test was done to help pinpoint where the variation
in mean values occurred. This test showed that the MLHR2
mean correlation coefficient was significantly different
than the BLHR value, but that there was no significant
difference between the BLHR mean value and the MLHR1 and
MLHR3 mean values.

6.3 Grid-point precipitation/LHR comparison

The correlation coefficient results reveal a
fundamental problem with this statistic. When the
precipitation is subgrid-scale in character, it is very
difficult for any computational scheme which uses grid-
scale data to specify LHR in sufficient detail to yield
high correlations. Thus, while various schemes may yield
LHR in appropriate regions, they likely will not match the
exact locations of the observed precipitation. As a
consequence, even though from a dynamical standpoint a
reasonable LHR distribution is presented, the correlation
coefficient may falsely indicate that the calculations are
of little value. This is indeed the situation at the

first three map times, when Fig.6.2 shows very poor
correlations but Figs.5.1 and 5.2 suggest a more favorable
comparison.

An alternate way of comparing LHR distributions is to
determine for a given area the total number of points at
which precipitation was observed and LHR was calculated at
each map time of the study. This compilation for the
total grid area is given in Table 6.3. These totals serve
to reinforce some earlier conclusions concerning the
changes in precipitation and LHR patterns with time. The
general expansion in these areas prior to 0300GMT is
clearly shown by the increase in the number of LHR grid
points within each field. The tendency for the MLHR1 and
MLHR3 modifications to increase the area of LHR(see
section 5.1.5) is shown by the larger number of points
where latent heating is calculated when compared with the
BLHR values. The decrease in the calculated latent heat
release area caused by the MLHR2 scheme is also seen in
Table 6.3. Clearly, gridpoint totals for the MLHR2 scheme
compare more closely with the observed precipitation
values than do the other computational schemes.

From a dynamical standpoint it is sufficient to
properly specify the LHR occurring within different air
mass regimes. The total area compilation given in Table
6.3 is useful for the first three map times because nearly
the entire grid area is influenced by the same air

Table 6.3. Total number of observed precipitation and calculated LHR points over the entire study area.

	1200GMT	1500GMT	1800GMT	PERIOD 1 AVG	2100GMT	0000GMT	0300GMT	0600GMT	PERIOD 2 AVG	TOTAL AVG
OBS PRECIP	23	16	21	20	50	60	65	72	62	35
BLHR	52	52	83	62	96	98	99	84	94	67
MLHR1	60	69	100	76	126	.109	109	87	108	94
MLHR2	24	23	30	26	59	68	81	59	67	49
MLHR3	71	94	82	82	112	106	121	105	111	99

mass(see Fig.3.1). However, at later map times the Gulf warm front moves northward and the cold front moves eastward with the result that the domain becomes influenced by three air masses. In order to tabulate grid point totals representative of each of these air masses the total grid was partitioned into three subregions, as shown in Fig.6.3. The Northeast subregion is defined as those grid points north of the warm front that developed at 0000GMT. The Southeast subregion is identified as that part of the grid south of the warm front, and the Western subregion encompasses the area behind the occluded/cold front. A simple count of the number of grid points where precipitation was observed and latent heat release was calculated in each subregion and for each map time is presented in Table 6.4. These statistics identify the extent to which LHR was reasonably represented in different air mass regions even if the precise location of that LHR was not correct when compared with the observed precipitation summaries. i.e., when poor correlations were obtained.

The transformation of the observed precipitation pattern from scattered convective areas to a highly organized synoptic-scale area is readily shown by comparing Periods 1 and 2. In Period 1(1200GMT-1800GMT) the number of points reporting observed precipitation was nearly the same for the three subregions. This is likely

WESTERN REGION

NORTHEAST REGION

SOUTHEAST REGION
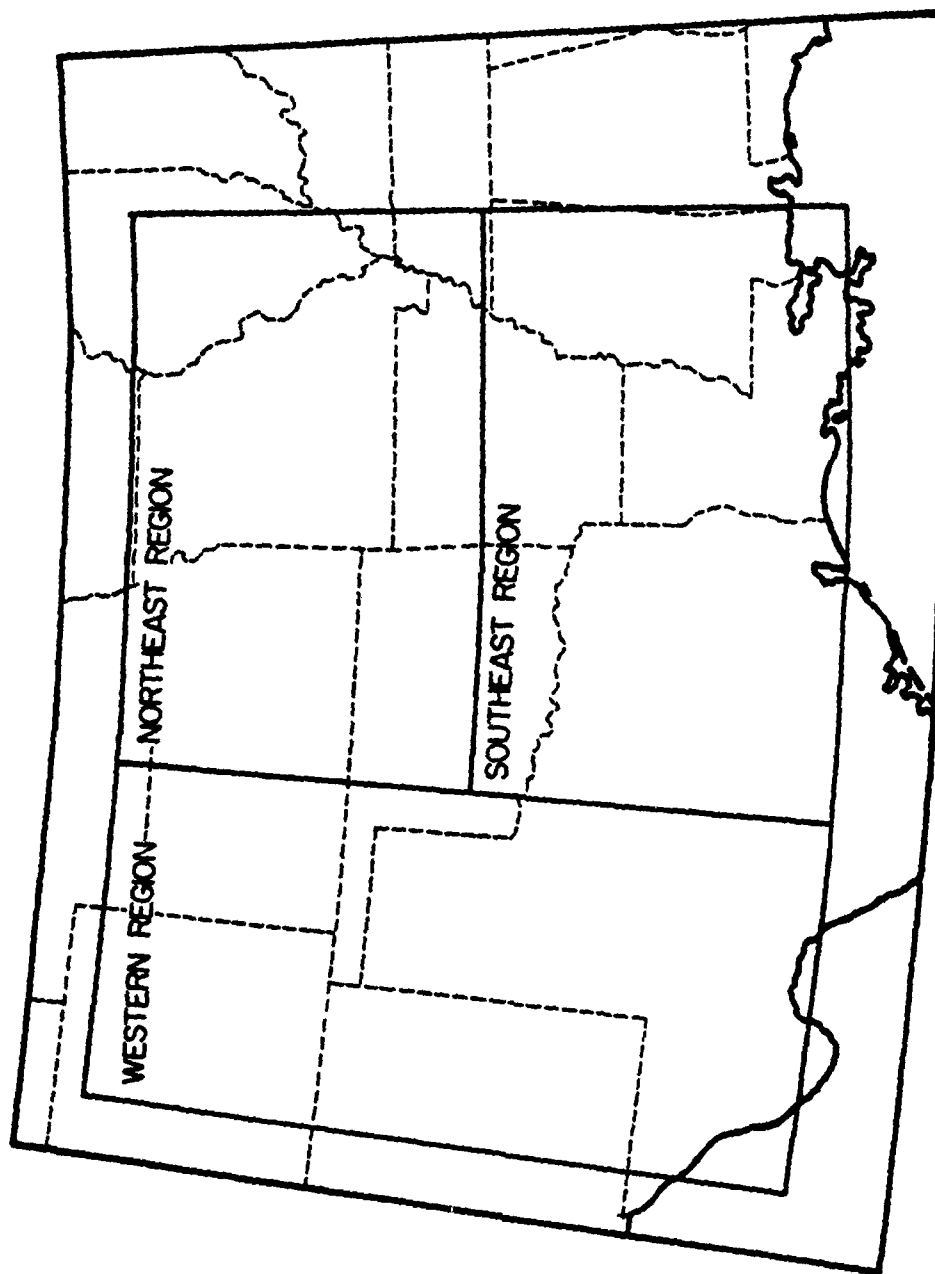
Figure 6.3. Subregions of the SESAME I grid.

Table 6.4. Total number of observed precipitation and calculated LHR points over the three subregions.

NORTHEAST SUBREGION (50 grid points)

	1200GMT	1500GMT	1800GMT	PERIOD 1 AVG	2100GMT	0000GMT	0300GMT	0600GMT	PERIOD 2 AVG	TOTAL AVG
OBS PRECIP	13	5	2	7	24	33	39	40	34	22
BLHR	17	20	26	21	26	40	39	40	36	30
MLHR1	29	24	31	28	40	50	50	48	47	39
MLHR2	14	3	4	7	12	38	43	37	33	22
MLHR3	35	42	27	35	34	50	50	50	46	41

SOUTHEAST SUBREGION (50 grid points)

	1200GMT	1500GMT	1800GMT	PERIOD 1 AVG	2100GMT	0000GMT	0300GMT	0600GMT	PERIOD 2 AVG	TOTAL AVG
OBS PRECIP	6	6	8	7	7	7	13	18	11	9
BLHR	25	13	24	21	34	27	30	27	30	26
MLHR1	9	13	27	16	44	25	28	22	30	24
MLHR2	5	0	12	6	21	11	17	12	15	11
MLHR3	9	18	19	15	38	21	31	22	28	22

WEST SUBREGION (60 grid points)

	1200GMT	1500GMT	1800GMT	PERIOD 1 AVG	2100GMT	0000GMT	0300GMT	0600GMT	PERIOD 2 AVG	TOTAL AVG
OBS PRECIP	7	5	11	8	19	20	13	14	17	13
BLHR	10	19	33	21	36	31	30	17	29	26
MLHR1	22	32	42	32	42	34	31	17	31	31
MLHR2	5	20	14	13	26	19	21	10	19	16
MLHR3	27	34	36	32	40	35	40	33	37	35

because all three subregions are influenced by the same air mass type during this period. As the cyclone developed and moved eastward, the Northeast subregion quickly gained predominance, with precipitation occurring at the majority of its 50 grid points. The other two subregions show only modest increases in observed precipitation coverage after 1800GMT. The movement of the cold front into central Texas after 0000GMT is shown by the decrease in total observed precipitation points in the Western subregion and an increase in the Southeastern subregion. This table also shows that the BLHR calculations did very well in matching the observed precipitation grid-point totals in the Northeastern region during Period 2. However, during Period 1 the BLHR totals are much greater than the observed precipitation summary indicates. This overestimation is also noted in the other subregions throughout the study period.

An evaluation of the total number of points where latent heat release is calculated by the modification schemes offers some interesting insights. In the Northeastern subregion the MLHR1 and MLHR3 schemes have more points than both the observed precipitation and BLHR at virtually every map time. The MLHR2 modification performs impressively in matching the number of observed precipitation points in this subregion throughout the study period.

In the Southeast subregion, on the whole, all of the modifications reduced the number of points where latent heating was calculated. Here again, the MLHR2 scheme did better in reproducing the total number of observed precipitation points. The movement of the cold front into this region is clear as the latent heating totals increase significantly during Period 2.

Finally, in the Western subregion the increase in the convective activity along the cold front as it moves through this region, followed by a decrease as the front exited the subregion after 0000GMT, shows up on all summaries. As in the other subregions, the MLHR2 scheme yields the most favorable comparison with the observed precipitation totals in both periods.

7.   SUMMARY AND CONCLUSIONS

This study has investigated the utilization of satellite imagery to modify conventional latent heat release estimates.   The SESAME I time period of 10-11 April 1979 provided a set of enhanced meteorological data which could be used to test the well established latent heat release parameterization technique described in section 2.3 and the use of satellite-derived cloud cover to modify these latent heating values.

An initial difficulty encountered in this study was to define a standard of comparison for the various latent heat release calculations. Initial evaluations compared maps of basic and modified LHR fields with hourly radar summaries; satellite-derived cloud cover; and gridded, temporally-averaged observed precipitation fields. Then the latter values were used for further evaluation in which area averages, correlation coefficients, and areal grid point totals were examined.   By combining these approaches a more complete picture of the LHR fields was obtained and the impact of the weaknesses identified in Section 4.1 for the individual comparative forms was lessened.

During the study period, a cyclone developed rapidly forcing an initially scattered precipitation pattern to become an organized synoptic-scale convective precipitation pattern after 1800GMT 10 April. As shown in the discussion in Chapters 4 and 5, the basic and modified LHR fields did reasonably well in capturing the general precipitation patterns shown in the radar and observed precipitation summaries in Period 1(1200GMT-1800GMT). Yet, poor correlation coefficients between the LHR estimates and observed precipitation values were obtained for this period. These low correlations were attributed to the inability of the LHR calculations to capture the exact location of the small-scale convection which dominated the study area during this early period. Still, it is important to note that the modifications did improve the LHR estimates obtained from the basic calculations. Better comparisons between the modified LHR and the radar and observed precipitation summaries, smaller differences between the area-averaged observed values and modified LHR, and improved correlation coefficients support this conclusion.

As the convection became more organized after 1800GMT, there was a large improvement in the BLHR calculations. This was noted in the qualitative evaluation but was especially apparent in the correlation coefficents. Correlations for the BLHR estimates increased from -0.05

at 1800GMT to 0.46 at 0600GMT. Here again, the modifications were able to improve on the performance of the BLHR calculations. Furthermore, correlations between observed precipitation and LHR calculations were consistently highest for the MLHR2 scheme.

Recognizing that the correlation coefficients depend on precise placement of calculated and observed values, a second pattern comparison procedure, which depends only on comparability over a general area, was devised. For this, the total grid area was divided into three subregions, each representative of a different air mass region after the cyclone and its frontal systems became well-developed. Within each subregion the number of points with observed precipitation or LHR were counted and compared. The overall tendency for the MLHR1 and MLHR3 schemes to increase the number of points where latent heating was calculated was readily apparent, as was the decrease in these LHR point totals resulting from the MLHR2 modification. The increase by the first and third modifications was due to their response to the cloud cover increase in advance of an approaching precipitation region and the tendency for these schemes to calculate LHR in areas of cloud that linger behind a departing precipitation region.

There is considerable support for identifying the MLHR2 scheme as being the modification that is most comparable

to the observational data forms. The use of the 235K threshold as a discriminator between convective and stable cloud regions was based on the success that Arkin(1979) had during GATE using this temperature to correlate fractional cloud cover and 6h rainfall accumulations. In the present qualitative evaluation the MLHR2 modification more consistently matched the precipitation pattern and the radar summaries than did the basic and the other two modified LHR fields. Furthermore, the vertical cross-sections derived from this modification, which had its greatest impact on the magnitudes of the convective LHR values, reduced the LHR estimates to magnitudes that were much more comparable to the vertical profiles of Fuelberg et al. (1985) and the vertical cross-sections of Robertson (1983).

The MLHR2 modification's departure from the area-averaged observed precipitation totals were similar in magnitude to the other schemes. However, the MLHR2 scheme had the highest correlation coefficients and the best overall percent improvement over the BLHR correlation coefficients(45%). Finally, the MLHR2 modification matched the number of observed precipitation points in the three subregions more closely than the other calculated values for nearly every map time used in this study.

The success of this modification is tempered by several key points. The first is that the MLHR2 scheme

The success of this modification is tempered by several key points. The first is that the MLHR2 scheme occassionally went too far in the elimination of LHR values at grid points. Although it clearly matched the radar summaries better. It underestimated the areal coverage of the observed precipitation fields at two map times(1200GMT and 1800GMT). Second, despite its positive affect on the BLHR values, it yielded area- averaged LHR totals which underestimated the observed precipitation values, especially in Period 2(2100GMT-0600GMT); and it was unable to produce good correlation coefficients during Period 1(1200GMT-1800GMT). A third point focuses on the nature of the particular synoptic-scale disturbance under study. This cyclone was a well-developed spring storm with a well-established regime of severe convection and associated clouds extending high into the atmosphere. In cases containing significant precipitation caused by convective clouds with tops predominantly warmer than 235K, this modification would eliminate much of the latent heating.

The methods used in this study to derive and modify latent heat release collectively represent a relatively simple approach to a very complex problem. While there is little doubt that the use of satellite imagery to improve LHR estimates shows merit, even more complex modifications using the approach of this study would seem unwarranted.

The movement from a single threshold enhancement to one with several thresholds often did not return a significant increase in the accuracy of the latent heating calculations. Although one can imagine that a new scheme could be devised which combines the discrimination between cloud type (convective or stable) with the identification of cloud level (low, middle, or high), this study's results hold out little hope that much improvement would result.

BIBLIOGRAPHY

BIBLIOGRAPHY

Alberty, R.L., D.W. Burgess, C.E. Hane, and J.F. Weaver, 1979: Project Severe Environmental Storms and Mesoscale Experiment: SESAME Operations Summary, 1979. NTIS Rep. No. NASA-TM-78256, National Technical Information Service, Springfield, Va., 365pp.

Anthes, R.A., 1977: A cumulus parameterization scheme utilizing a one-dimensional cloud model. Mon.Wea.Rev., 105, 270-286.

Arakawa,A.,and W. Chao, 1973: A cumulus parameterization scheme and its applications. Paper presented at the 8th Tech. Conf. on Hurricanes and Tropical Meteorology, Key Biscayne, May 14-17, Amer. Meteor. Soc.

Arkin, R.A., 1979: The relationship between fractional area coverage of high cloud and rainfall accumulations during GATE over the B-scale array. Mon.Wea.Rev., 107, 1382-1387.

Aubert, E.J., 1957: On the release of latent heat as a factor in large scale atmospheric motion. J.Meteor.,14, 527-542.

Barnes,S.L., 1964: A technique for maximizing details in numerical weather map analysis. J.Appl.Meteor.,3, 396-409.

_____, 1973: Mesoscale objective map analysis using weighted time series operations. NOAA Tech. Memo. ERL-NSSL-62, 60pp.

Barrett, E.C., 1970: The estimation of monthly rainfall from satellite data. Mon.Wea.Rev.,98, 322-327.

_____, 1971: The tropical Far East; ESSA satellite evaluations of high season climatic patterns. Geog.J.,137, 535-555.

_____, 1972: Geography from Space. Pergamon, Oxford, 98pp.

_____, and D.M. Martin, 1981: The Use of Satellite Data in Rainfall Monitoring, 1981 Academic Press, London, 340pp.

Carlson, T.M., R.A. Anthes, M. Schwartz, S.G. Benjamin, and D.G. Baldwin, 1980: Analysis and prediction of severe storms environment. Bull.Amer.Meteor. Soc.,61, 1018-1032.

Ceselski,B.F., 1973: A comparison of cumulus parameterization techniques. Tellus,25, 459-478.

Danard,M.B., 1964: On the influence of released latent heat on cyclone development. J.Appl.Meteor.,3, 27-37.

_____, 1966: On the contribution of released latent heat to changes in available potential energy. J.Appl. Meteor.,5, 81-84.

Donner, L.J. ,and K.L. Kuo, 1982: The significance of thermodynamic forcing by cumulus convection via the general circulation model. J.Atmos.Sci.,39, 2159-2181.

Edmon,H.J.,Jr. ,and D.G. Vincent, 1976: An application of two tropical parameterization schemes of convective latent heat release in midlatitudes. Mon.Wea.Rev.,104, 1141-1153.

Fuelberg,H.E.,M.G. Ruminski and D.O'C. Starr, 1985: Mesoscale generation of available potential energy in the warm sector of an extratropical cyclone. Mon.Wea.Rev.,113, 1150-1165.

Gerhard,M.L.,H.E. Fuelberg,S.F. Williams and R.E. Turner, 1979: AVE-SESAMEI: 25-mb sounding data. NTIS Rep.No. NASA-TM-78256, National Technical Information Service, Springfield, Va.,365pp.

Griffith,C.G.,W.L. Woodley,P.G. Grube, D.W. Martin,J. Stout and D.N. Sikdar, 1978: Rain estimation from geosynchronous satellite imagery-visible and infared studies. Mon.Wea.Rev.,106, 1153-1171.

_____,_____, S. Browner,J. Teijeiro,M. Maier,D.W. Martin,J. Stout ,and D.N. Skidar, 1976: Rainfall estimations from geosynchronous satellite imagery during daylight hours. NOAA Tech.Rep.ERL-356-WMPO 7, Boulder,Co., 106pp.

Gyakum,J.R., 1983a: On the evolution of the QE II storm I:Synoptic aspects. Mon.Wea.Rev.,111, 1137-1155.

_____, 1983b: On the evolution of the QE II storm II: Dynamic and thermodynamic structure. Mon. Wea.Rev.,111, 1156-1173.

Hicks,C.R., 1982: Fundamental Concepts in the Design of Experiments. CBS College Publishing,New York, 418pp.

Hildebrand, P.H.,N. Towery,and M.R. Snell, 1979: Measurement of convective mean rainfall over small areas using high-density raingauges and radar. J.Appl.Meteor.,18, 1316-1334.

Hill,K.,G.S. Wilson ,and R.E. Turner, 1979: NASA's participation in the AVE-SESAME '79 program. Bull.Amer.Meteor.Soc.,60, 1323-1329.

Hudlow,M.D.,R. Arkell,V. Patterson,P. Pytlowany, F. Richards ,and S. Geotis, 1979: Calibration and intercomparison of the GATE C-band radars. NOAA Tech.Rep. EPS 25, Center for Experiment Design and Data Analysis,NOAA, 78pp.

Kessler,E.III, 1969: On the distribution and continuity of water substance in atmospheric circulations. Meteor. Monogr., 32,Amer.Meteor.Soc., 84pp.

Krishnamurti,T.N. ,and W.J. Moxim, 1971: On
    parameterization of convective and non-convective
    latent heat release. J.Appl.Meteor.,2, 368-378.

_____. Ramanathan,N.L. Pan, R.J. Pasch ,and J.
    Molinari, 1980: Cumulus parameterization and rainfall
    rates I. Mon.Wea.Rev.,108, 465-472.

Kuo,H.L., 1965: On the formation and intensification of
    tropical cyclones through latent heat release by
    cumulus convection. J.Atmos.Sci.,22, 40-63.

_____, 1974: Further studies of the parameterization of
    the influence of cumulus convection on large- scale
    flow. J.Atmos.Sci.,31, 1232-1240.

Liang,W.J., 1978: The modification and application of
    Kuo's parameterization of cumulus convection in midd.e
    latitudes. NASA Contractor Report 2998, 90pp.

Lin,S.-C. ,and P.J. Smith, 1979: Diabatic heating and
    generation of available potential energy in a tornado
    producing extratropical cyclone. Mon.Wea.Rev.,107,
    1169-1183.

Lin,S.-J. ,and P.J. Smith, 1985: Utilization of satellite-
    derived cloud cover to improve the estimation of
    latent heat release in a winter extratropical cyclone.
    Mon.Wea.Rev., 113, 1942-1950.

Moore,J.T. and H.E. Fuelberg, 1981: A synoptic analysis of
    the first AVE-SESAME '79 period. Bull.Amer.
    Meteor.Soc.,62, 1577-1590.

Ng,C.Y., and Y.-T. Sheu, editors, 1985: Data catalog
    series for space science and applications flight
    missions, Volume 4a: Descriptions of meteorological
    and terrestrial applications spacecraft and
    investigations. NSSDC/WDC-A-R&S 85-03, 107pp.

O'Brien, J.J., 1970: Alternative solutions to the
    classical vertical velocity problem.
    J.Appl.Meteor.,9, 197-203.

Ooyama,K., 1971: A theory of parameterization of cumulus convection. J.Meteor.Soc.Japan,49, 744-756.

Orville,H.D. ,and F.J. Kopp, 1977: Numerical simulation of the life history of a hailstorm. J.Atmos.Soc., 34, 1596-1618.

Robertson,F.R., 1983: Cumulus-scale heating and its influence in meso-α dynamics during AVE/SESAME I. Preprints of the 13th Conference on Severe Local Storms, Tulsa, Ok., October 17-20,Amer.Meteor.Soc., 350-353.

_____, and P.J. Smith, 1983: The impact of moist processes on the energetics of extratropical cyclones. Mon.Wea.Rev.,111,723-744.

Scofield,R.A. ,and V.J. Oliver, 1977: A scheme for estimating convective rainfall from satellite imagery. NOAA Tech. Memo. NESS No.86, 47pp.

Seguin,W.R.,R.B. Crayton,P. Sabol ,and J.W. Carlile, 1978: GATE convection subprogram data center: Final report on ship surface data validation. NOAA Tech.Rep. EPS 25, Center for Experiment Design and Data Analysis,NOAA, 78pp.

Simpson,J. ,and V. Wiggert, 1971: 1968 Florida cumulus seeding experiment: numerical model results. Mon.Wea.Rev., 99, 87-118.

Smith, P.J., 1971: An analysis of kinematic vertical motions. Mon.Wea.Rev.,99, 715-724.

_____,P.M. Dare, and S.-J. Lin, 1984: The impact of latent heat release on synoptic-scale vertical motions and the development of an extratropical cyclone system. Mon.Wea. Rev.,112, 2421-2430.

Smith,E.A. ,and S.Q. Kidder, 1978: A multispectral satellite approach to rainfall estimates. Unpublished manuscript, Colorado State Univerity, Fort Collins, 26pp.

Takeda, T., 1971: Numerical simulation of a precipitating
    convective cloud: the formation of a long lasting
    cloud. J.Atmos. Sci.,28, 350-378.

Tracton,M.S., 1973: The role of cumulus convection in the
    development of extratropical cyclones.
    Mon.Wea.Rev.,101, 573-592.

Vincent,D.G.,G.B. Pant ,and H.J. Edmon,Jr., 1977:
    Generation of available potential energy of an
    extratropical cyclone system. Mon.Wea.Rev.,105, 1252-
    1265.

_____, and J.H. Homan, 1983: Mesoscale analysis of
    pressure and precipitation patterns during AVE-SESAME
    1979, 10-11 April. Bull.Amer.Meteor.Soc.,64, 23-28.

Weather Almanac, 1977. Edited by J.A. Ruffner and F.E.
    Bair, Gale Research Company. Detroit, Mi., 728pp.

Wilheit,T.T., 1972: The electrically scanning microwave
    radiometer(ESMR). Nimbus 5 Users Guide, NASA Goddard
    Space Flight Center, 55-105.

Woodley,W.L.,A.R. Olsen,A. Herndon ,and V. Wiggert, 1975:
    Comparison of gage and radar methods of convective
    rain measurement. J.Appl.Meteor.,14, 909-928.

_____,C.G. Griffith,J.S. Griffin, and S.C.
    Stromatt, 1980: The influence of GATE convective
    rainfall from SMS-1 imagery. J.Appl.Meteor.,19, 388-
    408.

END

DTIC

9 — 86